2003

# Imaging the complexity of an active normal fault system: The 1997 Colfiorito (central Italy) case study

L. Chiaraluce
*Istituto Nazionale di Geofisica e Vulcanologia*

W. L. Ellseworth
*U.S. Geological Survey*

C. Chiarabba
*Istituto Nazionale di Geofisica e Vulcanologia*

M. Cocco
*Istituto Nazionale di Geofisica e Vulcanologia*

JOURNAL OF GEOPHYSICAL RESEARCH, VOL. 108, NO. B6, 2294, doi:10.1029/2002JB002166, 2003

# Imaging the complexity of an active normal fault system: The 1997 Colfiorito (central Italy) case study

L. Chiaraluce[1]
Istituto Nazionale di Geofisica e Vulcanologia, Rome, Italy

W. L. Ellsworth
U.S. Geological Survey, Menlo Park, California, USA

C. Chiarabba and M. Cocco
Istituto Nazionale di Geofisica e Vulcanologia, Rome, Italy

Received 22 August 2002; revised 5 February 2003; accepted 27 February 2003; published 6 June 2003.

[1] Six moderate magnitude earthquakes ($5 < M_w < 6$) ruptured normal fault segments of the southern sector of the North Apennine belt (central Italy) in the 1997 Colfiorito earthquake sequence. We study the progressive activation of adjacent and nearby parallel faults of this complex normal fault system using ~1650 earthquake locations obtained by applying a double-difference location method, using travel time picks and waveform cross-correlation measurements. The lateral extent of the fault segments range from 5 to 10 km and make up a broad, ~45 km long, NW trending fault system. The geometry of each segment is quite simple and consists of planar faults gently dipping toward SW with an average dip of 40°–45°. The fault planes are not listric but maintain a constant dip through the entire seismogenic volume, down to 8 km depth. We observe the activation of faults on the hanging wall and the absence of seismicity in the footwall of the structure. The observed fault segmentation appears to be due to the lateral heterogeneity of the upper crust: preexisting thrusts inherited from Neogene's compressional tectonic intersect the active normal faults and control their maximum length. The stress tensor obtained by inverting the six main shock focal mechanisms of the sequence is in agreement with the tectonic stress active in the inner chain of the Apennine, revealing a clear NE trending extension direction. Aftershock focal mechanisms show a consistent extensional kinematics, 70% of which are mechanically consistent with the main shock stress field. *INDEX TERMS:* 7205 Seismology: Continental crust (1242); 7209 Seismology: Earthquake dynamics and mechanics; 7215 Seismology: Earthquake parameters; 7230 Seismology: Seismicity and seismotectonics; *KEYWORDS:* normal faults, segmentation, seismicity, double-difference location, stress inversion

**Citation:** Chiaraluce, L., W. L. Ellsworth, C. Chiarabba, and M. Cocco, Imaging the complexity of an active normal fault system: The 1997 Colfiorito (central Italy) case study, *J. Geophys. Res.*, *108*(B6), 2294, doi:10.1029/2002JB002166, 2003.

## 1. Introduction

[2] During September and October 1997, six earthquakes with $5 < M_w < 6$ struck the Umbria-Marche region (Figure 1) causing extensive damage and great concern in the population. After the beginning of the seismic sequence, a dense temporary local network was installed over the epicentral area, allowing us to collect a very high quality data set of digital waveforms. Details of the acquisition and preliminary earthquake locations for the $M_d > 2.5$ seismic events located with a 1-D velocity model are given by *Amato et al.* [1998] and *Deschamps et al.* [2000]. Seismological data and geodetic measurements were used to constrain kinematic source models, the upper crustal structure and the fault geometry of the largest magnitude earthquakes [see *Ekström et al.*, 1998; *Michelini et al.*, 2000; *Pino and Mazza*, 2000; *Capuano et al.*, 2000; *Salvi et al.*, 2000; *Chiarabba and Amato*, 2003; L. Chiaraluce et al., Complex normal faulting in the Apennines thrust-and-fold belt: The 1997–98 seismic sequence in central Italy, submitted to *Bulletin of the Seismological Society of America*, 2002, hereinafter referred to as Chiaraluce et al., submitted manuscript, 2002]. All the seismological observations are consistent with shallow, gently dipping blind normal faults. The lack of clear coseismic surface expressions of the main faults makes fault locations and geometry ambiguous [*Cinti et al.*, 1999; *Cello et al.*, 2000; *Basili and Meghraoui*, 2001]. There are still open questions concerning the role played by

[1] Also at Dip. di Scienze della Terra, Universita' degli Studi di Perugia, Perugia, Italy.


0148-0227/03/2002JB002166$09.00

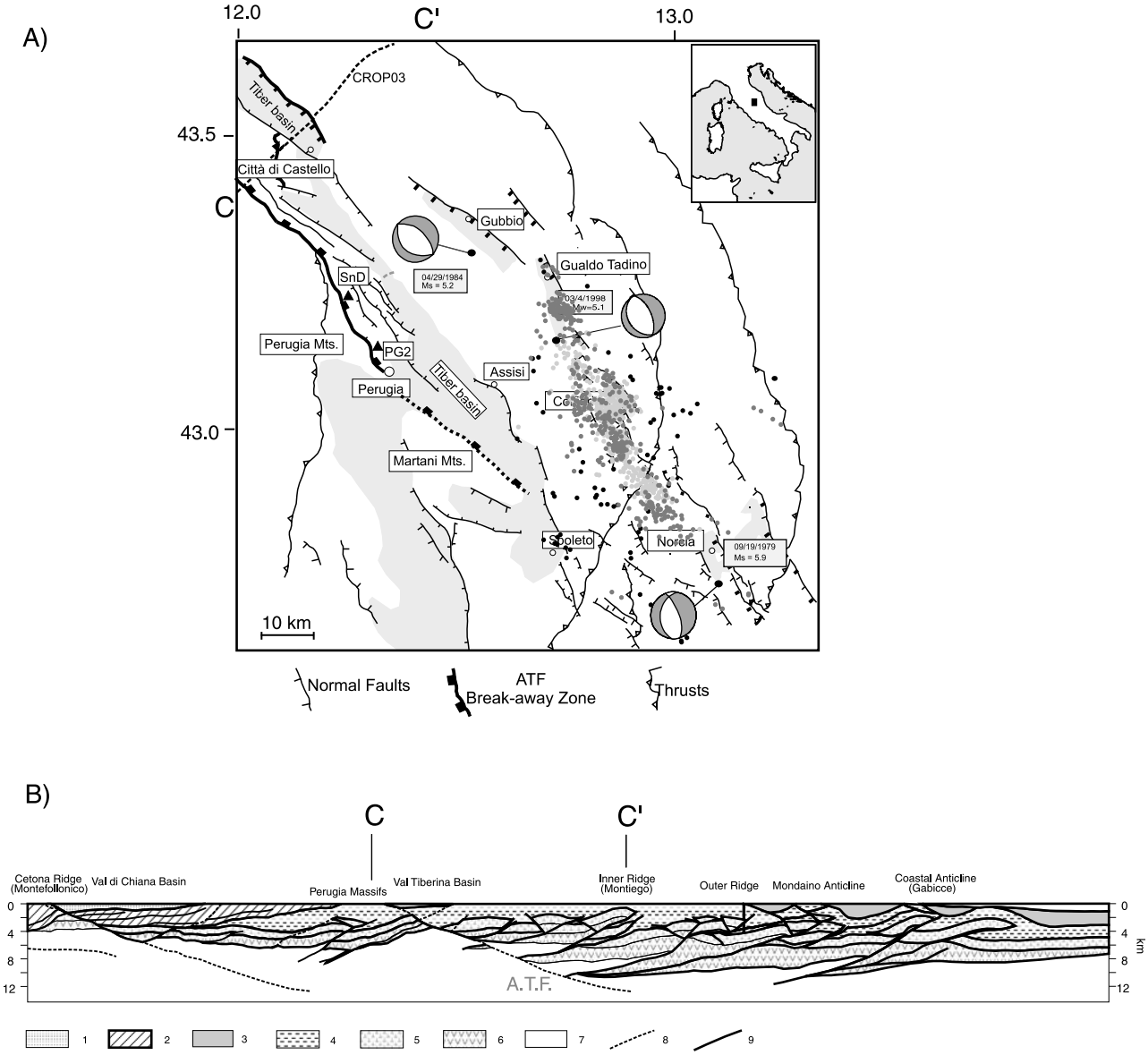


**Figure 1.** (a) Schematic structural map of the Umbria-Marche region simplified from *Barchi et al.* [2000], showing the major contractional and extensional faults. The focal mechanisms of the three other earthquakes ($M_w > 5$) that occurred in the region, respectively in 1984 (Gubbio area [*Haessler et al.*, 1988]), 1998 (Gualdo Tadino (Chiaraluce et al., submitted manuscript, 2002)), and 1979 (Norcia [*Deschamps et al.*, 1984]). In black, the seismicity recorded by the Italian National Network and relocated using the double-difference earthquake location algorithm that occurred from 1987 to the beginning of the Umbria-Marche sequence (26 September); in light gray from 26 September to 3 November and dark gray from 3 November to 2000. The shaded area indicates the Plio-Quaternary basins. (b) Geological interpretation of the seismic reflection line CROP03 from the Mount Cetone ridge to the Adriatic Sea [after *Barchi et al.*, 1998] (see part of the location in Figure 1a): 1, continental and shallow marine neoautochthonous successions; 2, Tuscan metamorphic and nonmetamorphic successions; 3, Plio-Pleistocene outer Marche turbidities; 4, Miocene Umbria-Marche turbidities, Oligo-Miocene marl subunit, Cretaceous-Eocene scaglia subunit; 5, Jurassic-Cretaceous Umbria-Marche carbonates; 6, Triassic Umbria-Marche evaporites; 7, basement in the strictest sense; 8, normal faults; 9, thrust faults. ATF indicates the Alto Tiberina Fault, which is a NE dipping normal fault.

the preexisting compressional structures on the evolution and geometry of Quaternary complex normal fault system and consequently on the deformation style of the northern Apennine.

[3] The detailed analysis of earthquake occurrence and fault interaction requires the accurate knowledge of the precise spatial location of earthquake hypocenters, especially in the case of blind crustal faults. This situation is

particularly common in the northern Apennines (Italy), where most of the seismogenic areas are characterized by low tectonic strain ($0.5 \times 10^{-7}$ yr$^{-1}$ [see *Hunstad et al.*, 2003]) and shallow blind faults. In general, for small events, earthquake location uncertainty is typically many times larger than the source dimension (i.e., 200 m to 1 km uncertainty compared to dimensions of 10 to 100 m for $M = 1-2$ earthquakes [*Waldhauser and Ellsworth*, 2000]), limiting the study of the fine fault geometry.

[4] In this paper we relocated about 1650 earthquakes with $2.5 < M < 6$, recorded over a period of 40 days, using the double-difference (DD) earthquake location algorithm [*Waldhauser and Ellsworth*, 2000; *Waldhauser*, 2001] that incorporates ordinary absolute travel time measurements and cross-correlation *P* and *S* wave differential travel time measurements. Many recent studies show that very accurate hypocentral determinations with errors of a few tens of meters can be obtained with cross correlation data. High-resolution images of faults may be enhanced along with the organization of the seismicity in time and space (i.e., Whittier Narrows earthquake by *Shearer* [1997], San Andreas Fault by *Rubin et al.* [1999], Hayward fault by *Waldhauser and Ellsworth* [2002], Calaveras fault by *Schaff et al.* [2002], and Long Valley Caldera by *Prejean et al.* [2002]). While most of the improvements described are for strike-slip faults, reverse faults or volcanic areas, only few normal fault systems have been studied so far. The literature concerning earthquake sequences occurred on normal faults is quite large (i.e., Norcia 1979, Irpinia 1980, and Gubbio 1984 in Italy; Borah Peak 1983 and Eureka Valley 1993, in the United States; Kalamata 1986, Kozani-Grevena 1995, and Athens 1999 in Greece), but it is poor in revealing the details of the fault geometry and general contentions as for example about normal fault listricity. The 1997 Colfiorito earthquake sequence in the complex tectonic setting of the North Apennine offers the possibility to unravel the anatomy of a normal fault system and to investigate fault segmentation.

[5] In this study we compute relative locations of aftershocks using the DD method starting from the 3-D earthquake locations calculated by *Chiarabba and Amato* [2003]. Therefore we use the spatiotemporal distribution of seismicity and fault plane solutions (the latter are taken from *Ekström et al.* [1998] and Chiaraluce et al. (submitted manuscript, 2002)) to identify active faults and to constrain their geometry. Finally, we compute the stress field from main shock focal mechanisms by using a stress tensor inversion and we compare it with the aftershock fault plane solutions.

## 2. Seismicity and Tectonic Setting

[6] The 1997 Colfiorito earthquake sequence is located in the Umbria-Marche region within the axial zone of the northern Apennines (Figure 1a). The area is characterized by the presence of a complex pattern of thrusts, folds and normal faults, reflecting the superposition of two main tectonic phases: an upper Miocene-lower Pliocene compressional phase forming E-NE verging thrusts and folds, and a coaxially superimposed Quaternary extensional phase, forming intramountain basins bounded by NNW-SSE trending normal faults which offset earlier fabrics.

[7] The sedimentary sequence involved in the thrust sheets consists of three major lithostructural units, from top to bottom: Meso-Cenozoic carbonates, Triassic evaporites (made up of alternated anhydrites and dolomites), and a Phyllitic Permian-Triassic basement. In the last fifteen years, the deep structure of the Umbria-Marche thrust and fold belt has been investigated by using commercial seismic reflection profiles [e.g., *Bally et al.*, 1986]. Deep boreholes and geophysical data show the involvement of the upper part of the basement during the compressional tectonic phase for the major thrust sheets [*Barchi et al.*, 1998]. Geological, geophysical and seismicity data integrated by *Mirabella and Pucci* [2001] and *Chiarabba and Amato* [2003], respectively, position the top of the basement under the Colfiorito basin at about 8 km depth.

[8] The contemporary NE trending extension of the northern Apennines [*Mariucci et al.*, 1999; *Frepoli and Amato*, 1997] is accommodated by low-angle ENE dipping normal faults that have been mapped at the surface [*Keller and Pialli*, 1990; *Keller et al.*, 1994; *Jolivet et al.*, 1998; *Rossetti et al.*, 1998] and are recognizable along the CROP03 deep seismic reflection profile [*Barchi et al.*, 1998], as well as by high angle antithetic normal fault systems (Figures 1a and 1b) [*Collettini*, 2001]. The Alto Tiberina Fault (ATF, see Figure 1), located in northern Umbria, represents the easternmost and the most recent ENE dipping low-angle normal faults of the northern Apennines. It borders the upper Pliocene-Quaternary continental Tiber basin (Figures 1a and 1b). The Umbria-Marche Apennines, located east of the Tiber basin, are affected by a set of active NW trending normal faults [*Barchi*, 2002], mapped at the surface with an average dip of $55°-70°$ dominating the topography [*D'Agostino et al.*, 2001], that border the continental Quaternary basins of Gubbio, Gualdo Tadino, Colfiorito and Norcia and intersect with older thrust faults. In the study area, the seismic profiles do not univocally reveal the presence of the ATF under the Colfiorito basin (dashed line in Figure 1a) and its presence is hypothesized on the base of regional geologic considerations [*Boncio et al.*, 2000; *Barchi et al.*, 2000]. Structural deformation models suggest a listric geometry for these high angle normal faults [*Bally et al.*, 1986; *Boncio and Lavecchia*, 2000; *Calamita et al.*, 2000; *Cello et al.*, 2000; *Barchi et al.*, 2000; *Meghraoui et al.*, 1999]. They are interpreted to flatten at depth and to steepen toward the surface.

[9] Within this portion of the belt, and close to the 1997 Colfiorito epicentral area, three other seismic sequences occurred in the past 20 years (Figure 1a), activating normal faults in the proximity of these Quaternary basins: the 1979 Norcia ($m_b$ 5.9) earthquake [see *Deschamps et al.*, 1984], the 1984 Perugia ($m_b$ 5.2) earthquake [see *Haessler et al.*, 1988], and the $M_L = 5.4$ Gualdo Tadino 1998 earthquake (see Chiaraluce et al., submitted manuscript, 2002). These seismic sequences appear to have activated SW dipping normal faults. As showed by *Deschamps et al.* [2000], the aftershock distribution of the 1979, 1984, and 1997–1998 earthquake sequences is almost continuous and follows the trend of the Apennines.

## 3. Earthquake Relocation Technique

[10] The DD algorithm can be applied when the hypocentral separation between two earthquakes is small com-

**Table 1.** One-Dimensional Velocity Model[a]

| Depth, km | *Vp* Velocity, km $s^{-1}$ | *Vs* Velocity, km $s^{-1}$ |
|---|---|---|
| 0–1.0 | 3.5 | 1.91 |
| 1.0–4.0 | 5.2 | 2.84 |
| 4.0–30.0 | 6.0 | 3.28 |
| >30 | 8.0 | 4.37 |

[a]Vp/Vs is constant and equal to 1.83.

pared to the source receiver separation. In this way, the ray paths between the source region and a common station can be considered similar along almost the entire ray path [*Frechèt*, 1985; *Got et al.*, 1994]. Therefore the difference in travel times for two events observed at one station can be attributed only to the spatial offset between the events [*Poupinet et al.*, 1984], and the latter can be computed with high accuracy by differencing Geiger's equation for earthquake location (see *Waldhauser and Ellsworth* [2000] for a comprehensive review). We combine *P* and *S* wave differential travel times derived from waveform cross correlation and *P* and *S* wave catalog travel time differences into a system of linear equations with each event pair (*k*, *l*) at each station (*i*) forming

$$\left[\frac{\delta t_{ik}}{\delta \mathbf{n}} - \frac{\delta t_{il}}{\delta \mathbf{n}}\right]\begin{bmatrix} \mathrm{r}_k \\ \mathrm{r}_l \end{bmatrix} = \left(dt_{ik}^{\mathrm{obs}} - dt_{ik}^{\mathrm{cal}}\right) - \left(dt_{il}^{\mathrm{obs}} - dt_{il}^{\mathrm{cal}}\right) \qquad (1)$$

where the **r** is the hypocentral adjustment vector and **n** is the 4 vector of Cartesian coordinates and origin time. A 1-D layered *P* velocity model for the area of investigation (Table 1) is used to compute the partial derivatives and $dt^{\mathrm{cal}}$ in equation (1). The velocity model is simplified from the 1D starting velocity model of *Chiarabba and Amato* [2003] coherently with rock velocities inferred from boreholes data [*Bally et al.*, 1986] and the *Vp/Vs* ratio equal to 1.83. Double difference equations are built to link each event to several neighbors, so that all events are connected and the solution for the adjustment to each hypocenter can simultaneously be determined. We use program hypoDD [*Waldhauser*, 2001] to compute the solution to equation (1). HypoDD solves equation (1) by weighted least squares (LSQR [*Paige and Saunders*, 1982]) using the conjugate gradients method. Improved hypocenters are found by iteratively adjusting the vector difference between hypocentral pairs. Hypocentral parameters and partial derivatives are updated after each iteration. Hypocentral errors are estimated by using the singular valued decomposition (SVD) to solve equation (1) [see *Waldhauser and Ellsworth*, 2001] for subsets of the earthquakes because error estimates obtained with LSQR are overly optimistic.

[11] The DD technique allows the use of any combination of ordinary phase picks from earthquake catalogues and/or high-precision differential travel times from phase correction of *P* and/or *S* waves. The former are expressed as differential travel times so that the same equation is used for all data. The combined use of both catalogue and cross-correlation data permits the simultaneous relocation of all events, with interevent distances within clusters of correlated events (multiplets) determined to the accuracy of the cross-correlation data, whereas relative locations between the multiplets and uncorrelated events are determined to the accuracy of the arrival times data.

### 3.1. Catalogue Travel Time Differences

[12] *P* and *S* wave arrival times from about 2000 local earthquakes of the 1997 seismic sequence have been carefully read on digital waveforms, assigning weights proportionally to reading uncertainty [see *Deschamps et al.*, 2000]. Data from seven stations of the Italian National Network (RSNC) located within 120 km from the area were added to the data derived from the 30 local stations. Pick quality of 0, 1, 2, 3 and 4 are used (reading errors <0.02 s, between 0.02 and 0.05 s, 0.05–0.08 s, 0.08–0.1 s, and more than 0.1 s, respectively). The starting hypocentral locations are those computed by using a three-dimensional model [see *Chiarabba and Amato*, 2003].

### 3.2. Cross-Correlation Travel Time Differentials

[13] In addition to the catalogue travel time differences, we measured travel time differentials for each event pair with waveforms that correlated at a common station using the cross-correlation method in the time domain described by *Schaff* [2001]. Waveform similarity decreases with event pair separation because of the increasingly different wave propagation paths and/or focal mechanisms, and generally breaks down after a separation distance exceeds roughly the first Fresnel zone (i.e., approximately 300 m for 5 Hz *P* waves).

[14] We considered similar two waveforms within a tapered 2.56 s (256 samples) window recorded at a specific station when both cross-correlation coefficients above 70% and mean coherence above 70% [*Schaff*, 2001] (see an example of similar waveforms in Figure 2). The distribution of coherency values for measured *P* and *S* wave differential travel times are shown in Figure 3. Both distributions feature a peak at 0.8 coherency, indicating the high quality of the data.

### 3.3. Parameters Setting and Data Weighting

[15] The choice of events to explicitly link in the design matrix of equation (1) can be adjusted in program hypoDD to define weak and strong neighbors that are differently weighted in the inversion. Moreover, the catalogue data are down weighted by a factor of 100 relative to the cross-correlation data after a few iterations [see *Waldhauser and Ellsworth*, 2000; *Waldhauser*, 2001]. Cross-correlation data are a priori weighted by the correlation coefficient, catalogue data by weights of 1, 0.75, 0.5, 0.25 and 0.1 for corresponding 0, 1, 2, 3 and 4 pick quality, respectively. Equal weights are used for *P* and *S* wave cross-correlation data. Residuals are reweighted after each iteration according to the misfit and the distance between events [see *Waldhauser and Ellsworth*, 2000, Figure 4]. Catalogue and cross-correlation data are removed/reweighted for event pairs with separation distances larger than/smaller than 10 and 2 km, respectively. Weights are highest for closest events and drop exponentially with increasing separation distance. Residuals larger than 6 times the median absolute deviation from the median of each data type are considered outliers and discarded.

[16] When using both data types simultaneously, one has to be aware that the first motion arrival times image the point of rupture initiation (hypocenter), whereas cross-correlation data image the center of moment release (hypo-

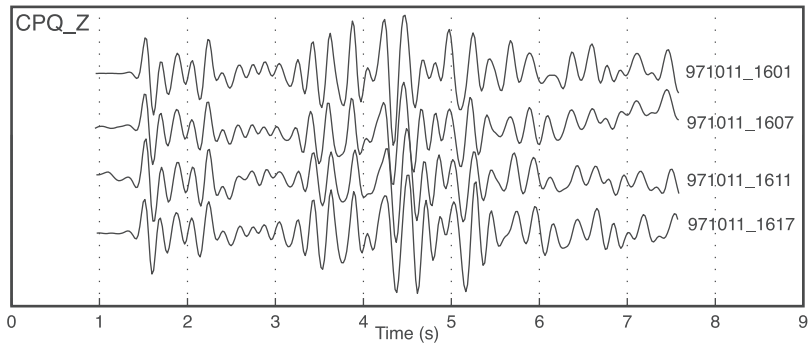


**Figure 2.** Example of seismograms (multiplets) recorded at the station CPQ containing *P* and *S* wave trains. We perform the cross-correlation analysis within a tapered 2.56 s window containing the *P* and *S* wave trains.

centroid) as the cross spectra of entire *P* or *S* phases are used to estimate the time delays between the event arrivals [*Waldhauser and Ellsworth*, 2000]. This observation should not create problems because we mostly cross correlate waveforms of small events and the difference in between hypocenter and hypocentroid should be of the same order of magnitude as the error in location.

## 4. Relocation Results

[17] From the initial set of earthquakes, we located 1650 events that occurred between 26 September and 3 November 1997. The average RMS error is 0.03 s and formal errors computed in the SVD mode are 70 m, 85 m and 120 m, respectively, in latitude, longitude, and depth. Consequently, structural details with dimensions of about 100 m can be reliably interpreted. We have also relocated the 3 September $M_L$ 4.2 foreshock, but could not relocate its early aftershocks, or the two main shocks of the 26 September, due to the small number of seismic stations that were operating at that time. The location error for these events is several hundred of meters.

[18] In Figures 4a and 4b we compare the tomographic locations obtained by *Chiarabba and Amato* [2003] with the hypoDD locations. We observe a significant improvement in focal depth, particularly in the peripheral areas. This allows us to better constrain the fault geometry at the ends of the main activated segments. The aftershock alignment now clearly depicts the dip of the fault, as evident in the NE-SW cross sections drawn for the southern area (Figure 4b). It is interesting to note that the location displacements seem to be systematic, mostly toward the east and NE and larger where the station coverage is poorest.

[19] Relocation results for all 1650 events appear in map view in Figures 5 and 6, and in a set of 18 vertical cross sections in Figure 7. The cross sections have been drawn perpendicular to the average strike of the main structures (NE-SW). Each cross section contains seismicity within 1 km of the section line. Figure 5 divides the sequence by time to identify those aftershocks that occurred after each of the six main earthquakes. In the next section we present the earthquake relocations and the temporal evolution of the sequence in order to constrain the fine geometry of the normal fault system.

### 4.1. Fine Geometry of the Normal Fault System

[20] The Umbria-Marche seismic sequence began on 3 September with a $M_w$ = 4.5 foreshock (event 1 in Figure 5) [see *Amato et al.*, 1998; *Ripepe et al.*, 2000]. The foreshock (black star) occurred midway between the two main events of 26 September (red stars) and at a shallower depth (4 km). The two 26 September events with $M_w$ = 5.8 (event 2) and

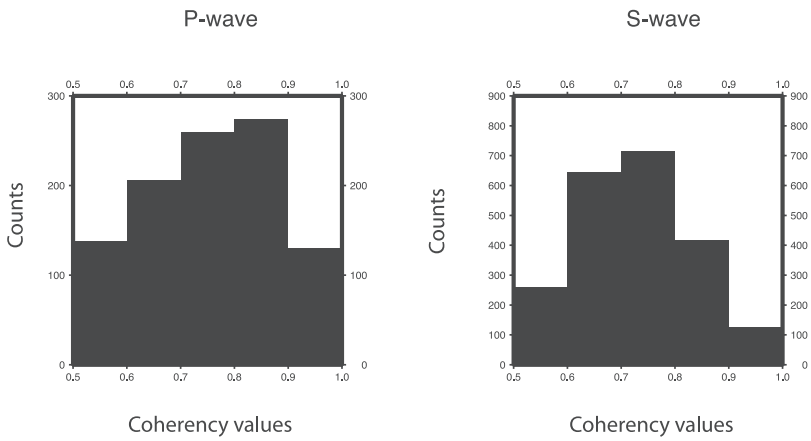


**Figure 3.** Quality of cross-correlation data. Histograms of coherency values of *P* and *S* phases used to determine travel times differences between events at common stations.

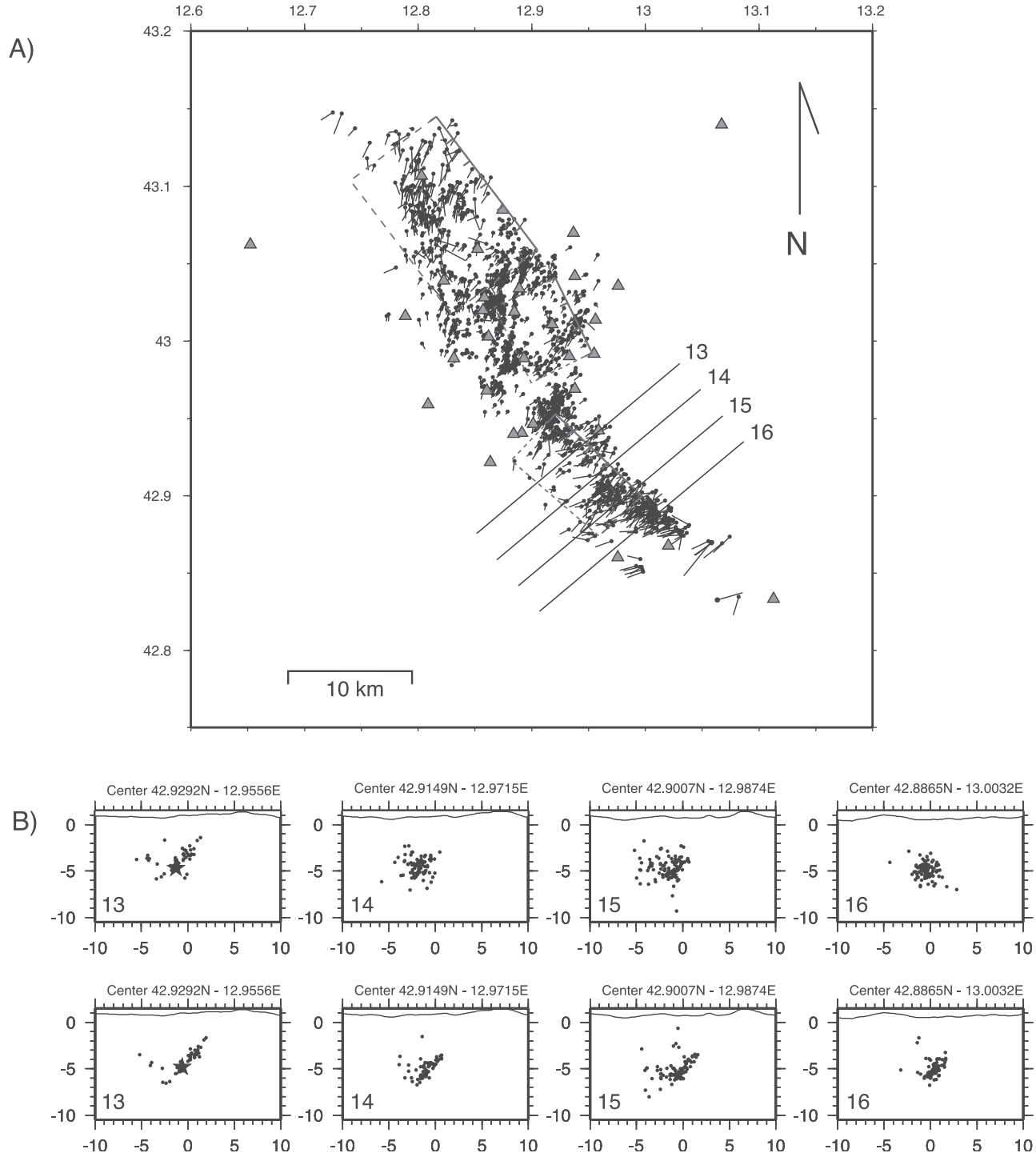


**Figure 4.** (a) Displacement vectors (black lines) between the 3-D locations obtained by *Chiarabba and Amato* [2003] using seismic tomography, and by the double-difference locations obtained with program hypoDD [*Waldhauser*, 2001] (black points). The triangles represent the seismic stations. (b) Set of four vertical cross sections. *Chiarabba and Amato* [2003] at the top and DD at the bottom. The star is the hypocenter of the 14 October main shock (event 7, see text for explanation).

$M_w$ = 6.0 (event 3) occurred within 9 hours of each other and within about 3 km of distance of one another. Both these events nucleated near the base of the seismogenic volume at 5.7 km of depth (see sections 6 and 7 in Figure 7 and Table 2). The aftershock distribution clearly depicts the two fault planes with a constant dip of ~35°–40° to the SW (see sections from 4 to 7 in Figure 7). A rough estimate of the width of the aftershock zones is close to 500 m. The modeling of both regional [*Pino et al.*, 1999] and strong motion [*Zollo et al.*, 1999] waveforms revealed clear evidence of unilateral rupture directivity in opposite directions along the strike of the fault planes: event 2 toward the

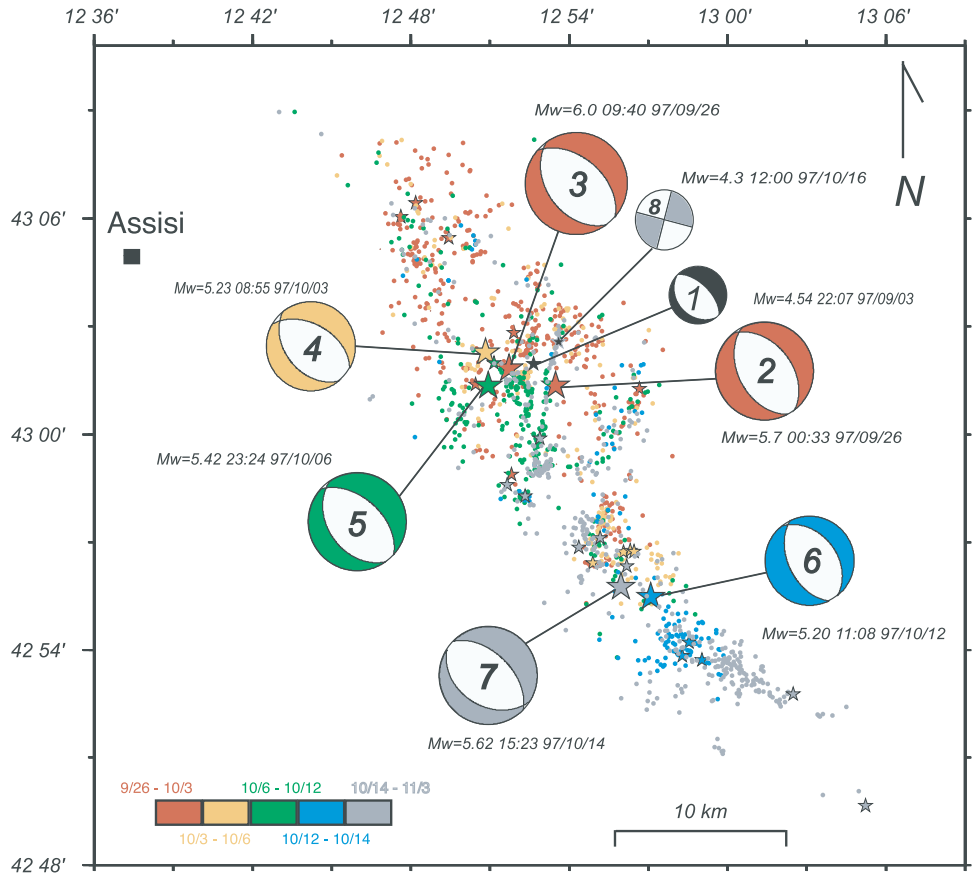


**Figure 5.** Map view of the relocated seismicity with focal mechanisms of the main events of the Umbria-Marche 1997 seismic sequence. The epicenters are color coded by time intervals defined by the six main shocks. Numbers in the focal sphere are sequential in time.

SE and event 3 toward the NW. The lack of aftershocks toward the NW and SE direction, for event 3 and 2 respectively agrees with unilateral rupture propagation. The fault corresponding to event 2 is clearly visible in the three sections to the SE (sections 7, 8, and 9 in Figure 7) for a length of ~5–6 km, while the fault plane of event 3 is visible in the sections to the NW (sections 3, 4, 5, and 6) for about 8–9 km. This latter structure seems to disappear to the NW, where in sections 2 and 3 the seismicity starts to be disperse over a volume. In this area, *Cattaneo et al.* [2000] located a $M_L$ 4.7 event, that occurred only seven minutes after the 26 September 0940 UT main shock (event 3), and used this location to constrain the maximum length of the main event. We estimate a total fault length for event 3 from aftershock distribution as not larger than 10 km.

[21] A few days, later two other shocks struck the same central area: the first on 3 October ($M_w$ = 5.2 event 4, yellow star in Figure 5) and the second on 6 October ($M_w$ = 5.4 event 5, green star in Figure 5). The event 4 nucleated at 4.7 km depth and had few aftershocks (yellow points in Figure 5). In sections 5 and 6 of Figure 7 we observe that the seismicity delineates only one main plane. This observation suggests that this earthquake occurred on the main shock (event 3) fault plane and ruptured a slip-deficit patch left unbroken by the previous event. Event 5 nucleated at 5.4 km of depth, and its related seismicity is shallower (see section 7, 8, and 9) than its hypocenter. Rupture propagated unilaterally toward SE (green points in Figure 5) [*Pino and Mazza*, 2000]. The activated fault has a planar geometry and it is positioned on the hanging wall of the structures that ruptured during the 26 September main shocks. There is a good agreement between the strike shown by the aftershock alignment and the strike resulting from the CMT solutions for all the largest events except for the 6 October (event 5). This event is also the only one for which the fault plane solution computed from polarity data is not consistent with the CMT focal mechanism (Figure 8). The former is slightly steeper and shows a left-lateral component larger than that shown by the CMT solution. We observe that the elongation of aftershock hypocenters of event 5 is striking almost N-S (350°) consistently with the plane of the first motion solution (see gray line in Figure 9).

[22] Between 3 and 6 October, the seismicity started to migrate toward the SE (Figure 5). The southern termination of the event 2 fault (section 11 in Figure 7) is characterized both by diffuse seismicity and by the occurrence of four earthquakes with $4.2 < M < 4.6$ (see Table 2) during this three days period. In section 11 of Figure 7 we have no clear evidence of a fault plane, while in sections 12 and 13 we see a plane dipping 40° to the SW, which is the fault plane that will rupture during the two subsequent earthquakes of 12 and 14 October. This fault plane is clearly activated before those large magnitude ($M > 5$) earthquakes. In fact, plotting only the seismicity that occurred during the 30 hours after

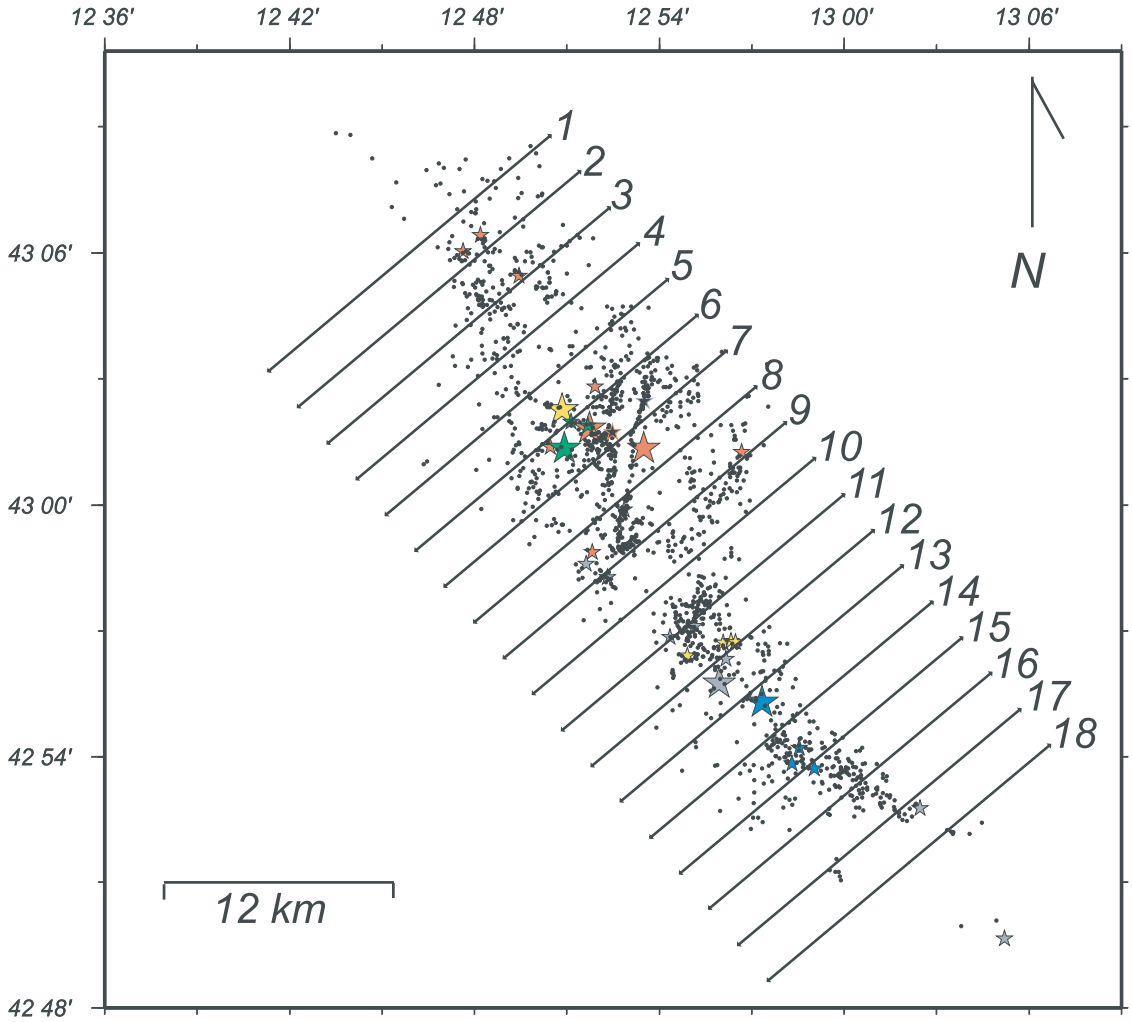


**Figure 6.** Map view of the seismicity of the sequence and the center lines of 18 vertical cross sections (NE-SW oriented) reported in Figure 7. The stars epicenters of events with $M > 4$ (see Table 2).

the first of these $M > 4$ events (occurred 4 October, 0649 UT), in Figure 10 we observe a clear fault plane dipping in the SW direction, which is very thin and with the main shocks positioned at the base, also in section 11. It is worth noting that only few hours of seismicity after moderate magnitude ($4.2 < M < 4.6$) events allow us to see the fault plane that will rupture within a week. This is a very nice example of activation and stress migration on a fault system imaged by very high quality seismicity data.

[23] In the following days the seismicity continued to migrate to the south where the $M_w = 5.2$ (event 6, blue star in Figure 5) and the $M_w = 5.6$ (event 7, gray star in Figure 5) occurred on 12 and 14 October, respectively. The seismicity related to events 6 and 7 shows only one main fault segment. The first event nucleated at 4.8 km and the second at 5.8 km depth, at the base of the seismogenic volume. These two main events are on the same well resolved fault plane that shows a constant dip to the SW of ~40°–45°.

[24] It is interesting to note that after 6 October in the northern sector seismicity clusters on well defined shallow NS structures located in between the two main shocks of 26 September, where on 16 October a $M_w = 4.3$ earthquake nucleated at 1 km depth (Figure 11). From aftershock distribution and focal mechanisms we infer the activation of a very shallow N-S oriented left-lateral strike-slip fault with a sequence of aftershock showing the same kinematics. The aftershocks are distributed within the upper 2–3 km of depth, for a length of ~6 km, and a width of ~100 m. In Figure 11 we observe, both in map view and in section, a second parallel strike-slip fault. Part of this strike-slip fault was activated between 6 and 12 October (Figure 5), after the occurrence of event 5 that, following our solution, showed a left-lateral strike-slip component. We will discuss the relationship between this earthquake and the surrounding faults in section 6.

[25] By the beginning of November 1997, the earthquake sequence had activated an area ~45 km long and 15 km of wide along the Apennines. The seismicity was confined within the upper 8 km depth. Most of the main events ($4.2 < M < 6$) are located at the base of their own aftershock sequences that delineate clear fault planes. The coseismic deformation is accommodated by several normal fault segments dipping to the SW and through minor normal faults or very shallow (nearly vertical) strike-slip faults within the overlap zones between adjacent segments. We did not find any evidence of seismicity either along antithetic faults

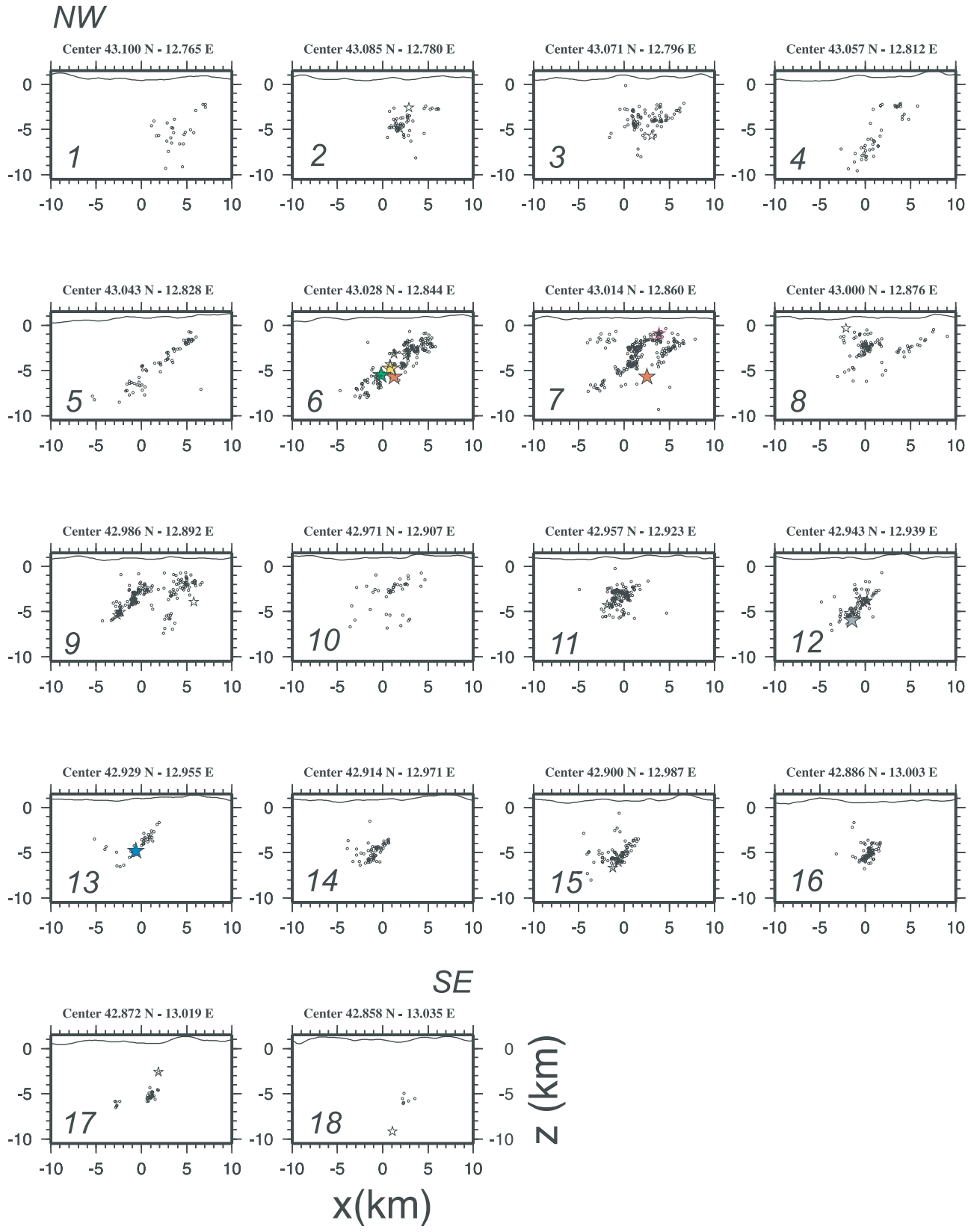


**Figure 7.** Set of 18 2-km-thick vertical cross sections identified in Figure 6. The stars are hypocenters of the main events ($4 < M < 6$).

**Table 2.** Location, Magnitude, and Focal Mechanism Parameters of the Main Events of the Sequence[a]

| No. | Latitude | Longitude | Depth, km | $M_w$ | Date | | | Time, UT | Strike | Dip | Rake |
|---|---|---|---|---|---|---|---|---|---|---|---|
| 1 | 12.8786 | 43.0118 | 4 | 4.54 | 3 | Sept. | 1997 | 2207 | 137° | 30° | 292° |
| 2 | 12.8917 | 43.0225 | 5.7 | 5.66 | 26 | Sept. | 1997 | 0033 | 152° | 46° | 277° |
| 3 | 12.8622 | 43.0305 | 5.7 | 5.99 | 26 | Sept. | 1997 | 0940 | 142° | 39° | 273° |
| | 12.8032[b] | 43.1068[b] | 2.6[b] | 4.7[b] | 26 | Sept. | 1997 | 0947 | | | |
| | 12.9447 | 43.0208 | 3.9 | 4.3 | 26 | Sept. | 1997 | 1330 | | | |
| | 12.8243 | 43.0907 | 5.7 | 4.3 | 27 | Sept. | 1997 | 0808 | | | |
| | 12.8412 | 43.0229 | 5.73 | 4.0 | 27 | Sept. | 1997 | 1713 | | | |
| | 12.8652 | 43.0468 | 3.3 | 4.0 | 27 | Sept. | 1997 | 1956 | | | |
| | 12.8639 | 42.9810 | 0.34 | 3.7 | 28 | Sept. | 1997 | 1124 | | | |
| | 12.794 | 43.1005 | 4.89 | 4.1 | 2 | Oct. | 1997 | 1059 | | | |
| 4 | 12.8475 | 43.0379 | 4.81 | 5.2 | 3 | Oct. | 1997 | 0855 | 141° | 43° | 286° |
| | 12.9151 | 42.9399 | 5.17 | 4.2 | 4 | Oct. | 1997 | 0649 | | | |
| | 12.9347 | 42.9451 | 4.02 | 4.2 | 4 | Oct. | 1997 | 1507 | | | |
| | 12.9389 | 42.9457 | 3.85 | 4.6 | 4 | Oct. | 1997 | 1613 | | | |
| | 12.9412 | 42.9453 | 3.8 | 4.1 | 4 | Oct. | 1997 | 1847 | | | |
| 5 | 12.8486 | 43.0226 | 5.51 | 5.4 | 6 | Oct. | 1997 | 2324 | 145° | 40° | 280° |
| | | | | | | | | | 170°[c] | 45°[c] | 310°[c] |
| | 12.8523 | 43.0328 | 4.31 | 4.2 | 7 | Oct. | 1997 | 0124 | | | |
| | 12.8615 | 43.0312 | 3.15 | 4.4 | 7 | Oct. | 1997 | 0509 | | | |
| 6 | 12.9517 | 42.9241 | 4.83 | 5.2 | 12 | Oct. | 1997 | 1108 | 154° | 51° | 278° |
| | 12.984 | 42.895 | 6.07 | 4.0 | 12 | Oct. | 1997 | 2131 | | | |
| | 12.9757 | 42.9033 | 5.76 | 4.0 | 13 | Oct. | 1997 | 1101 | | | |
| | 12.9719 | 42.8971 | 6.69 | 4.1 | 13 | Oct. | 1997 | 1309 | | | |
| 7 | 12.9325 | 42.9292 | 5.97 | 5.62 | 14 | Oct. | 1997 | 1523 | 122° | 38° | 260° |
| | 12.9057 | 42.9473 | 4.29 | 4.0 | 14 | Oct. | 1997 | 1624 | | | |
| | 12.8721 | 42.9710 | 5.02 | 4.2 | 14 | Oct. | 1997 | 2323 | | | |
| | 12.9362 | 42.9386 | 3.59 | 4.1 | 15 | Oct. | 1997 | 2253 | | | |
| 8 | 12.892 | 43.0411 | 0.94 | 4.4 | 16 | Oct. | 1997 | 1200 | 287° | 80° | 175° |
| | 12.9191 | 42.9517 | 2.98 | 4.0 | 16 | Oct. | 1997 | 0452 | | | |
| | 13.0412 | 42.8793 | 2.61 | 4.0 | 16 | Oct. | 1997 | 1731 | | | |
| | 12.8606 | 42.9765 | 5.38 | 4.1 | 19 | Oct. | 1997 | 1600 | | | |
| | 12.881 | 42.9979 | 2.58 | 3.3 | 20 | Oct. | 1997 | 0127 | | | |
| | 13.0869 | 42.8274 | 9.17 | 4.1 | 25 | Oct. | 1997 | 0308 | | | |

[a]Strike, dip, and rake angles are taken from the CMT solutions calculated by Ekstrom et al. (1998) unless otherwise noted.
[b]*Cattaneo et al.* [2000].
[c]Values obtained with polarity data and the FPFIT code in this study.

dipping to the NE or in the footwall of the system (see Figure 9). We do not observe any flattening of the seismicity with depth. Also for events with $4 < M < 5$, early aftershocks occurring in a few hours after the main event cluster on small normal fault segments SW dipping and with constant dip of ~40°.

## 5. Stress Inversion and Kinematics

[26] The 1997 Umbria-Marche seismic sequence is characterized by a strong similarity of fault plane solutions either for the main shocks or for the aftershocks: 70% (of the 321 available aftershock solutions) show normal faulting, while 24% and 6% have strike-slip and reverse mechanisms, respectively (see Figure 12a and Chiaraluce et al. (submitted manuscript, 2002)). The six largest events occur on normal faults, dipping to the SW. Their mechanisms agree with those of the earthquakes occurring before the 1997 sequence and recorded by the permanent Italian National Seismic Network (see Figure 1 and *Frepoli and Amato* [1997]). This suggests a homogeneous regional tectonic stress field in this section of the Apen-

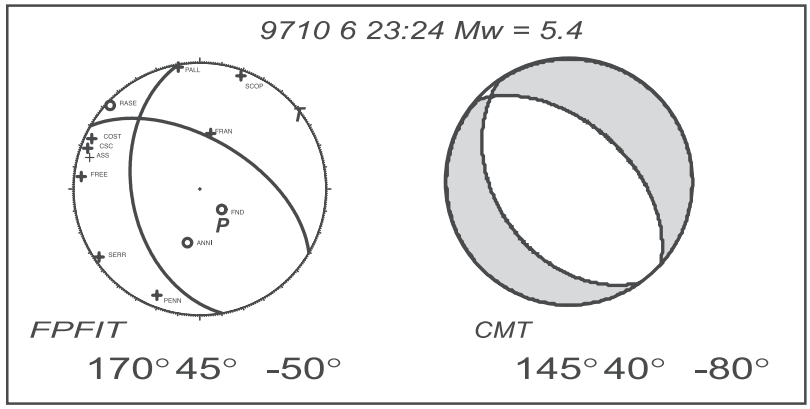


**Figure 8.** Focal mechanism computed by (left) polarity data and (right) the CMT for the 6 October $M_w$ = 5.4 earthquake.

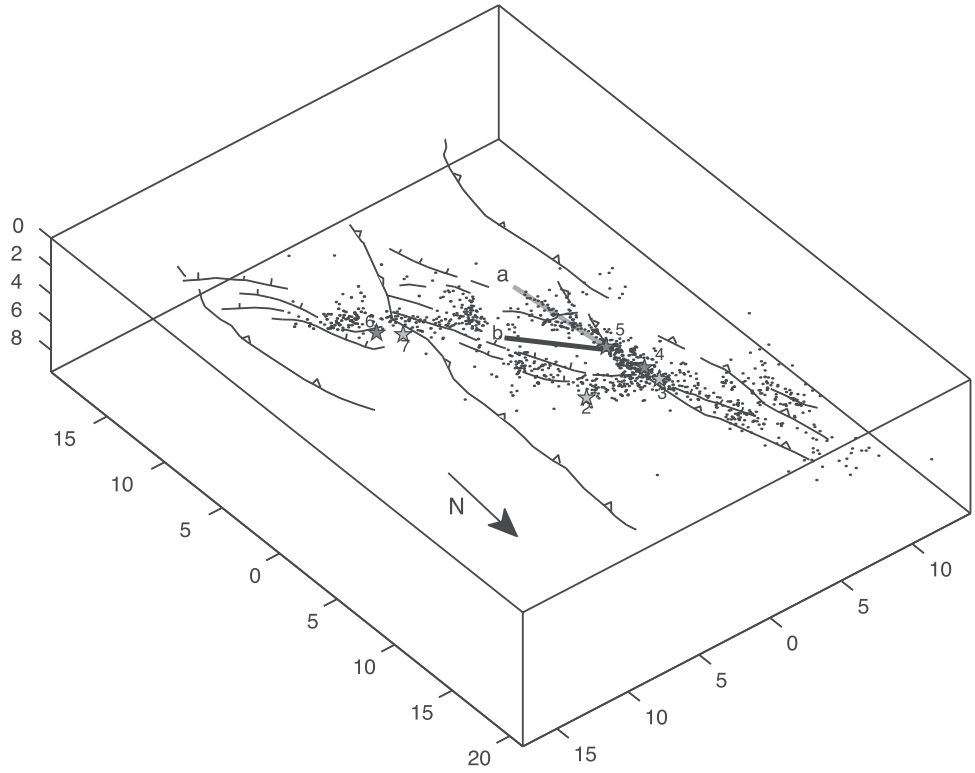


**Figure 9.** Orthographic view of Colfiorito sequence from NE and from an elevation of 40° showing the 1650 relocated seismic events. Stars represent the main earthquake hypocenters. The gray (line a) and black (line b) lines are the strike of the FPFIT and CMT solutions, respectively, for event 5. Normal and thrust faults are derived from *Calamita and Pizzi* [1994].

nines with the horizontal extension perpendicular to the chain.

[27] The details inferred about this complex fault system from the DD locations allow us to examine the uniformity of the focal mechanisms in terms of the local tectonic setting and fault interaction. To this end we perform both a stress tensor inversion from the main shock fault plane solutions and a forward modeling of aftershock mechanisms. We applied the *Michael* [1984] technique to the six largest magnitude ($M > 5$) events of the sequence to infer the regional tectonic stress field. We assume that the main shocks release an important unknown fraction of the tectonic stress acting on the fault plane. According to the *Michael* [1984] method, we also assume that the slip vector on average is parallel to the shear stress. Therefore we use the main shock stress field to test its compatibility with the aftershocks fault geometry and faulting mechanisms by comparing the observed aftershock slip vectors with the state of stress derived from the stress inversion [see *Michael et al.*, 1990]. Because we are able to distinguish the fault plane between the two nodal planes we treat them as slickensides in our stress tensor calculation.

[28] We use the CMT fault plane solutions for all six main shocks with $M > 5$, except for the 6 October earthquake for which we use the solution inferred from polarity data since it better agrees with its aftershock distribution. Despite the small number and the similarity of the fault planes, we obtain a well-constrained stress tensor (Figure 13a), with a misfit $\beta = 6.4$ (see *Michael* [1984] for a discussion on misfit). We find a subvertical $\sigma_1$, $\sigma_2$ subhorizontal and oriented along the strike of the fault system (NW-SE) and a subhorizontal $\sigma_3$ trending NE-SW. The $\phi$ [$= \sigma_2 - \sigma_3 / \sigma_1 - \sigma_3$] value is 0.6. The obtained stress tensor is in agreement with the stress field inferred by *Mariucci et al.* [1999] and *Frepoli and Amato* [1997] for the northern Apennines using borehole breakout and focal mechanisms inversion of background seismicity.

[29] In order to test if the computed tectonic stress, inferred from the largest shocks, is compatible with the aftershocks fault plane solutions, we project the stress tensor onto the nodal planes of the aftershock focal mechanisms (shown in Figures 12a and 12b) from Chiaraluce et al. (submitted manuscript, 2002). These focal mechanisms have a mean standard deviation in strike, dip, and rake of 10°, 15°, and 30°, respectively. We use the angular difference between the shear traction direction and the slip vector as a measure of the consistency between the applied stress tensor and the aftershock mechanism. A histogram of the difference appears in Figure 14 (gray columns). Because the 90% of the selected fault plane solutions have an error in rake less than 30° (see the black columns in Figure 14), we consider the aftershock focal solutions to be in agreement with the regional stress tensor when the angular difference is smaller. By this criterion, more than 70% of the aftershocks are consistent with the stress tensor shown in Figure 13a.

[30] It is important to note that among the 30% of the mechanisms inconsistent with the inferred stress field, 80%

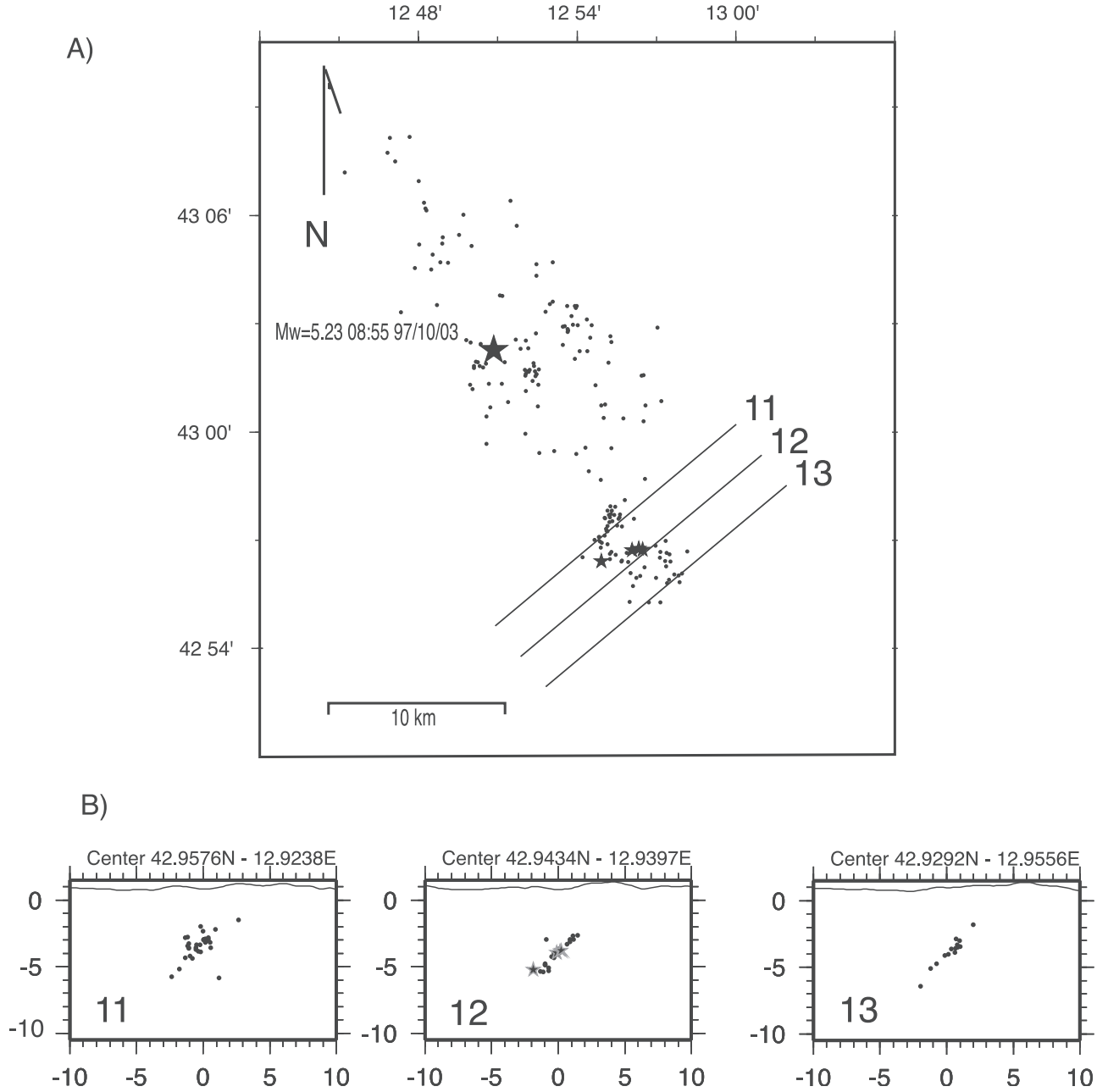


**Figure 10.** Seismic activity over a 30 hour time window in a map view and in three vertical sections starting with the origin time of the first of 4 events with $4.1 < M_w < 4.6$ (small gray stars) that occurred in the southern zone on 4 October (0649 UT). These events signed the migration of seismicity into the southern zone and, despite the short time window, clearly image several fault planes. We include the hypocenter of the 3 October event for comparison.

of them (about 24% of the total) occur on the shallow strike-slip faults. Most of these events activated shallow, N-S oriented structures, coincident with a portion of an inherited thrust, and therefore they occur on a distinct secondary structure. We propose that these events have been promoted (i.e., triggered) by the stress perturbations caused by the largest normal faulting earthquakes. A complete demonstration of this assertion is beyond the goals of the present study and will require accurate modeling of stress transfer. We point out here that the shallow strike-slip structures, striking about N10°, dipping 90° and with an average rake of 180°, are mechanically consistent with the retrieved orientation of the extensional axis $\sigma_3$ (N53°). Moreover, the parameter R resulting from our stress inversion suggests that $\sigma_1$ is larger than $\sigma_2$, but their difference is not very large. Therefore we speculate that these events might have been caused by coseismic stress transfer. Including the largest strike-slip event (occurred on 16 October) in the stress inversion does not change the retrieved stress field.

[31] Only about 6% of the total of the aftershock fault plane solutions are not explained by the proposed stress

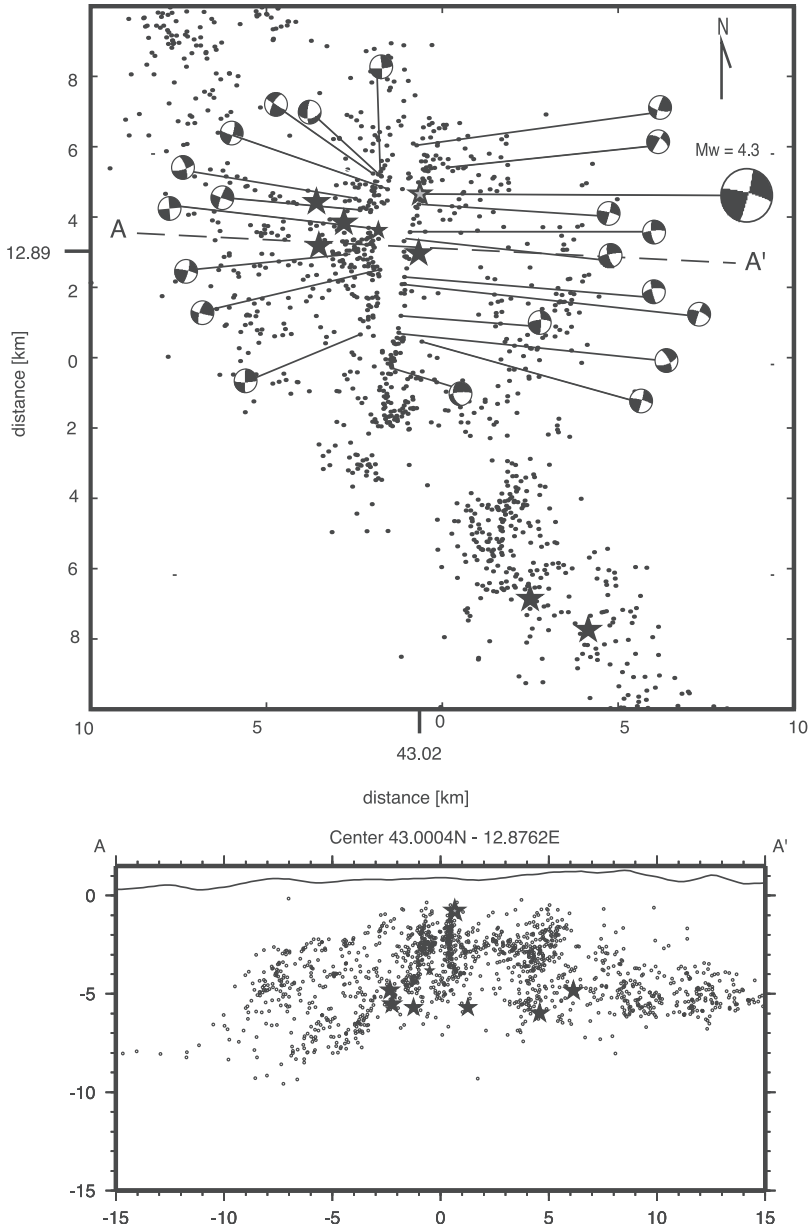


**Figure 11.** (top) Map view of the central area of the sequence and (bottom) vertical cross section along A–A′. In the cross section, the alignment of shallow (0–3 km) hypocenters along the north striking strike-slip faults is clearly visible.

field. These events are located in the top 4 km, have reverse or oblique fault plane solutions, and do not show any particular pattern. Therefore we conclude that a uniform stress field can explain the kinematics of most of the aftershocks and stress transfer and/or fluid flow might have played an important role in fault reactivation controlling earthquake locations and faulting mechanisms.

[32] We also determined a stress tensor by inverting the aftershock fault plane solutions (Figure 13b). The comparison between the stress tensor inferred from the main shocks (Figure 13a) with that one calculated from the aftershocks confirms that in the investigated area $\sigma_3$ is subhorizontal and oriented NE-SW and that the small difference in the plunge of $\sigma_1$ is due to the reactivation of preexisting fault planes as left-lateral strike-slip faults during the aftershock sequence. Our results suggest that most of the aftershocks are consistent with a uniform stress field.

## 6. Fault Model

[33] The seismicity relocated in this study and the surface traces of the main geologic structures (Plio-Quaternary normal faults and Neogene thrusts) derived from *Calamita and Pizzi* [1994] appear in orthographic projection in Figure 9. The view direction looks down from NE direction from an elevation angle of 40° (from the surface), corresponding to the average dip angle of the normal faults activated during the sequence. This figure clearly shows that the seismicity during the Colfiorito sequence is aligned along the strike direction of mapped normal faults. These

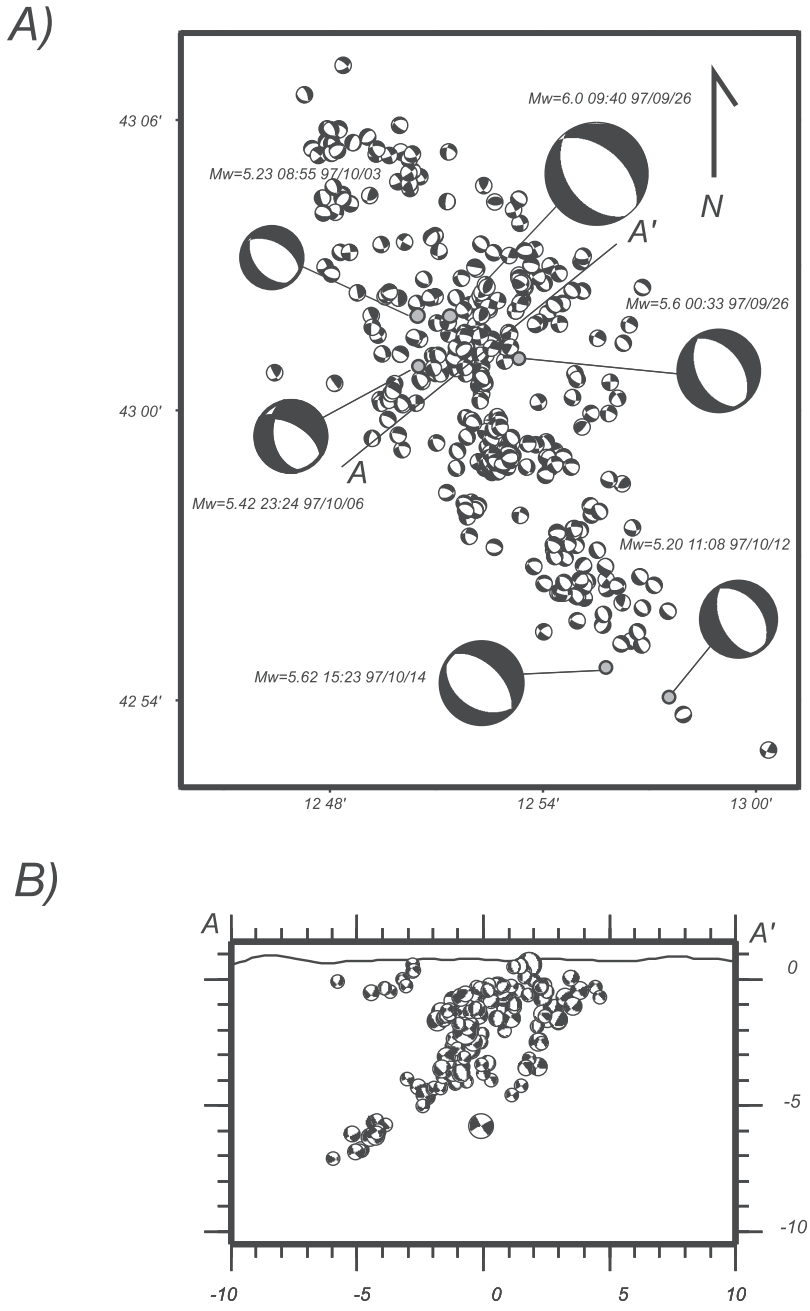


**Figure 12.** (a) Focal mechanism solutions of a selected subset of 330 aftershocks with $2.5 < M < 5$ on a map view. (b) NE-SW vertical cross section along A–A′.

faults are, in turn, segmented by previous N-S compressional structures. At the surface, the normal faults dip 60°–70° toward SW. All the main shocks (stars in Figure 9) nucleate very close to the intersection between the thrusts and the normal faults. Moreover, aftershocks off the main fault planes occur in the hanging wall of the normal faults. There is little evidence for seismic activity in the footwall.

[34] In this section we aim to construct a synoptic representation of the Colfiorito fault system. To this end we use the CMT fault plane solutions for the largest events (Table 2) and the first-motion polarity mechanism for event 5, as well as the aftershock distribution discussed in the previous sections. We fix the position and the dimension of each major fault plane using the information on rupture directivity [see *Pino and Mazza*, 2000] and, when available, the results of geodetic and waveform modeling studies [*Hunstad et al.*, 1999; *Salvi et al.*, 2000; *Capuano et al.*, 2000]. The size of the main fault planes have been scaled by the moment magnitude derived from *Ekström et al.* [1998] using a stress drop of 3 MPa.

[35] Figure 15 shows the fault model proposed in this study. The main normal fault segments are separated by the old thrust planes. Thus fault segmentation model and rupture behavior seem to be controlled by the lateral heterogeneity of the upper crust due to the intersection of the north trending inherited thrusts and the younger exten-

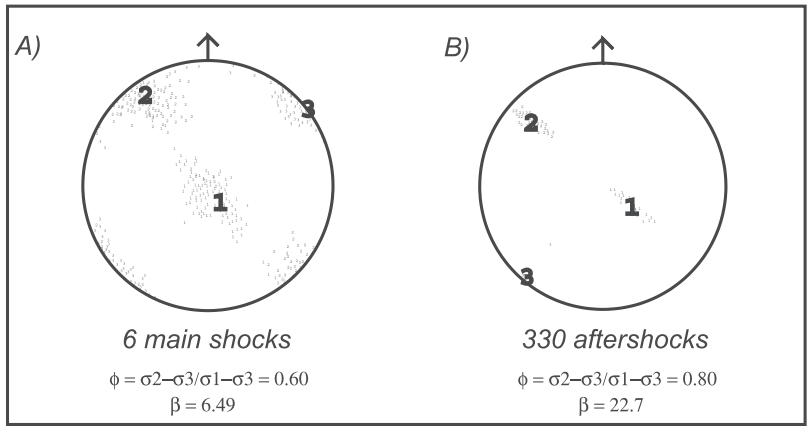


**Figure 13.** Stress tensor and 95% confidence regions [*Michael*, 1984] obtained from the inversion of (a) the fault planes of the six main shocks and (b) focal mechanism solutions of the aftershocks.

sional NW trending normal faults. In the central area, the two main shocks of 26 September (events 2 and 3) nucleated with about 3 km of each other and propagated in opposite directions. A left-lateral step of 3–5 km separates these two hypocenters, which has also been observed by seismic tomography [*Chiarabba and Amato*, 2003]. While all the main fault planes are in a good agreement with the strike of the mapped Quaternary normal faults, the seismicity related to event 5 is located below a lateral ramp thrust segment. This suggests that this portion of the thrust plane was reactivated due to stress transfer as also indicated by the strike-slip component observed in the focal mechanism of event 5. Moreover, the same north trending thrust segment has been reactivated at shallow depths (0–3 km) with pure strike-slip faulting episodes (see event 8 in Figure 15). We conclude that the segmentation, the rupture behavior of the major earthquakes and the maximum length of the active normal faults are controlled by preexisting inherited compressional structures. As observed in many other areas (e.g., see *Braunmiller et al.* [1995] for Klamath Falls Oregon and *Massonet and Feigl* [1995] and *Ichinose et al.* [1998] for Eureka Valley), we observe the initiation and termination of earthquake ruptures at geometrical barriers, in agreement with the interpretations of surface observations proposed by *Cinti et al.* [2000].

## 7. Discussion and Conclusions

[36] The accurate relative location of aftershocks performed in this study using the DD algorithm and cross-correlation measurement of digital data allow us to retrieve a very detailed picture of the Colfiorito normal fault system, imaging a complex pattern of small segments activated by moderate magnitude earthquakes. Normal faulting on SW dipping (40°–45°) planar rupture planes is constrained by aftershock distribution and focal mechanism analysis. The comparison of earthquake locations and surface geology reveals a segmented 45 km long NW trending fault system. The seismicity is confined within the first 8 km of the crust and above the Phyllitic Permian-Triassic basement.

[37] In Figure 16 we compare the distribution of 1650 aftershocks ($2.5 < M < 4.6$) and fault planes with the slip patterns proposed by *Hernandez et al.* [1999] for the three largest events and obtained by inverting GPS, InSAR and strong motion data. The largest shocks nucleated near the base of the seismogenic zone (5–6 km) and propagate

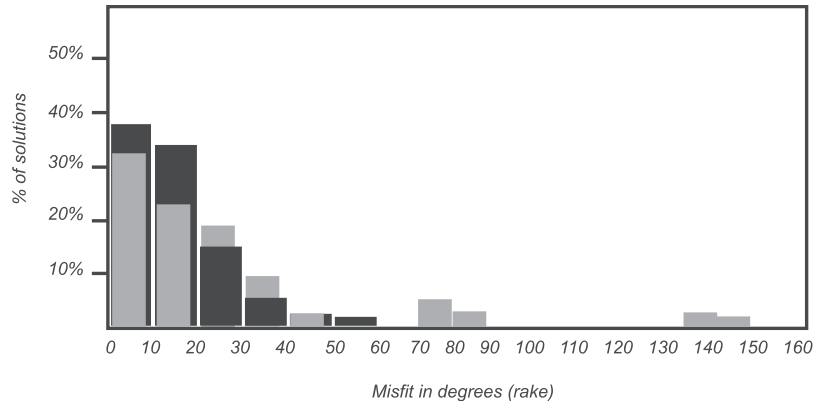


**Figure 14.** Composite histogram showing the mean standard deviation in rake for the FPFIT aftershock focal mechanism solutions (black). Angular difference (misfit) between the observed and the predicted rake applying the stress tensor on the strike and dip of each nodal plane of the aftershocks (gray).

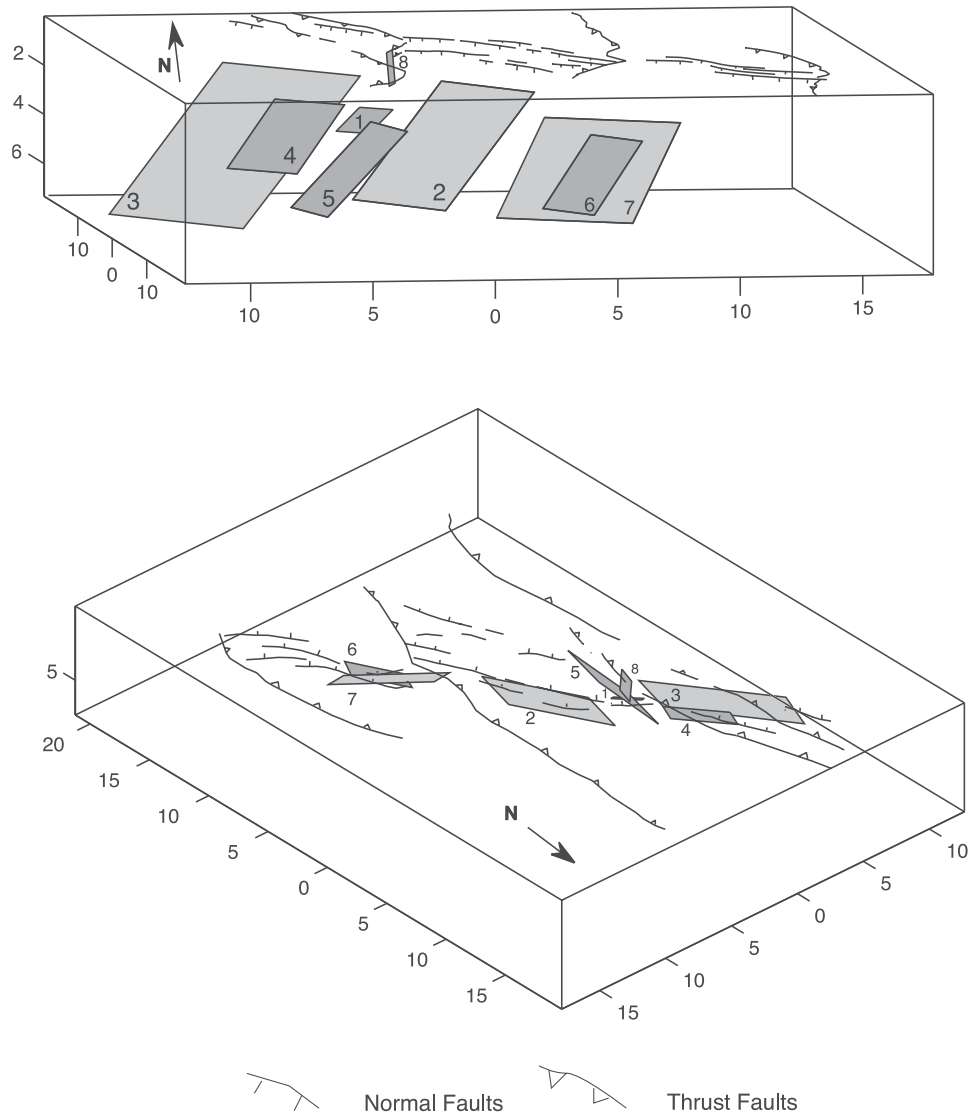


**Figure 15.** Synoptic representation of the Umbria-Marche fault system. Shaded squares represent the fault planes ruptures during the main faulting episodes, scaled for seismic moment with a stress drop of 3 MPa and position based on the hypocenter and rupture directivity [*Pino et al.*, 1999] information. Mapped normal and thrust faults are derived from *Calamita and Pizzi* [1994]. (top) View direction along the trend of the thrust faults; (bottom) view direction down dip direction of normal faults.

unilaterally and updip. Each large event had its own aftershock sequence on its fault plane upon which the aftershocks focal mechanisms are very similar to the main shock CMT solutions. Main shock rupture areas derived from both rupture directivity and slip distributions are characterized by the lack of aftershocks, in agreement with the anticorrelation of slip and aftershocks seen elsewhere [e.g., *Mendoza and Hartzell*, 1988]. We also observe that inherited compressional structures controls the segmentation of the NW trending Quaternary active normal faults.

[38] This model for this complex normal fault system helps us better understand the extensional deformation style and the tectonic setting of this section of the northern Apennines. Our results shed clear light on the present-day active tectonics of the area and the relationship between the faults at depth and the traces observed at the surface [see *Cello et al.*, 2000; *Cinti et al.*, 1999; *Meghraoui et al.*, 1999; *Barchi et al.*, 2000; *Chiarabba and Amato*, 2003]. One of the most interesting results is that all the activated segments maintain a planar geometry, without any flattening or evidence for listricity at depth, in agreement with earlier seismological and geodetic interpretations [see *Jackson and White*, 1989; *Braunmiller and Nàbelek*, 1996]. The fault planes cut the upper crust, from about 1 km down to 8 km depth, and aftershocks occur over a less than 0.5 km wide region around the proposed fault planes. Structural deformation models, based on surface geology and on the interpretations of seismic reflection profile, propose a listric geometry for the SW dipping, active normal faults of the northern Apennines [*Bally et al.*, 1986; *Barchi et al.*, 1998, 2000; *Boncio and Lavecchia*, 2000; *Meghraoui et al.*, 1999]. We have shown that the surface traces are positioned

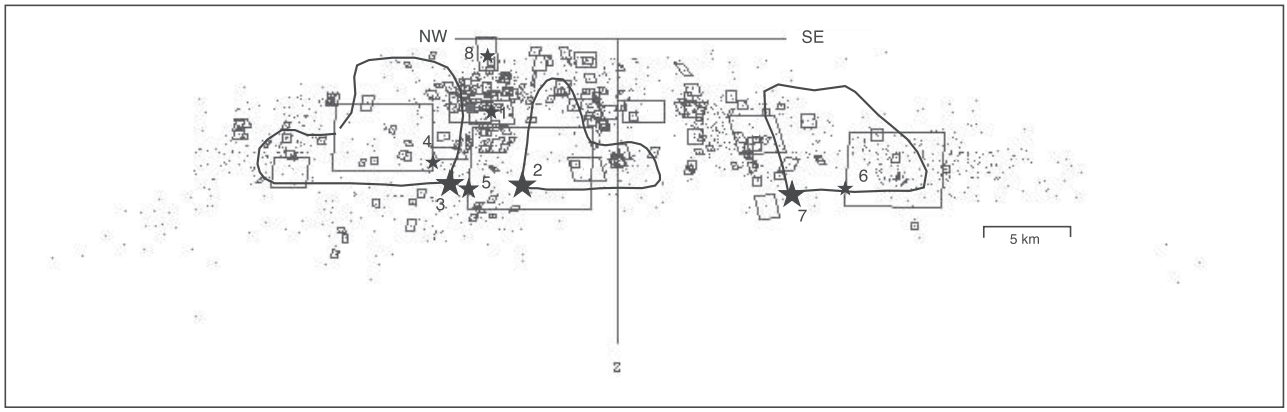


**Figure 16.** Vertical cross section of the aftershock distribution viewed from the SW. Projected aftershock planes are also shown (3 MPa stress drop). Contour of the slip patterns proposed by *Hernandez et al.* [1999] obtained inverting GPS, InSAR, and strong motion data for the three main events (2, 3, and 7). Fault model based on the rupture directivity, $M_w$ and fault plane solutions for the others large events (1, 4, 5, 6, and 8) from Figure 15.

just above the termination of the fault planes defined by the aftershocks whose upper tips remain deeper than 1 km of depth. The Colfiorito active faults seems to die at around 1 km depth, as revealed by aftershock and slip distribution during the main shocks. Only the fault that ruptured during the 26 September main shock ($M_w$ = 6.0, event 3 in Figure 5) seems to be shallower than 1 km according to geodetic data modeling [see *Hunstad et al.*, 1999; *Salvi et al.*, 2000]. In any case, the steeper (50°–70°) fault planes observed at the surface seems not to be the direct expression of the coseismic rupture at depth, but they might just accommodate the induced deformation in the weak upper 1 km of the crust.

[39] The depth termination of the activated seismogenic volume could be related to the Alto Tiberina fault (ATF in Figures 1a and 1b), which dips at low angle to the E-NE. Recent seismological observations have shown that, in the northern section of the study area (see the position of the CROP03 profile in Figure 1a) near Città di Castello, the ATF is active and thousand of microearthquakes ($0 < M_L <$ 2.8 and few $2.8 < M_L < 3.2$) have been recorded and located at depths ranging from 1 km to 8 km [*Piccinini and CDC Working Group*, 2002]. The microseismicity images a low angle (15°–20°) east dipping plane in the Città di Castello area. Going toward the southeast direction, below the Colfiorito area the ATF should become nearly subhorizontal. We did not locate any earthquake on a east dipping plane during the 1997–1998 Colfiorito sequence. However, the deepest subhorizontal portion of the ATF fault below the Colfiorito normal fault system could not be visible without locating microearthquakes with magnitudes much smaller than 2.5, which represents the magnitude threshold of the seismicity analyzed in this study. At depth greater than 8 km, corresponding to the top of the Phyllilitc Basement, the extensional deformation might also be accommodated by creep. Microseismicity due to creeping phenomena has been proposed to activate E-NE low angle dipping normal faults in an extensional tectonic setting with vertical $\sigma_1$ characterized by extremely vigorous and widespread nonvolcanic fluxes of $CO_2$ derived from mantle degassing and hence representing a continuous supply of fluids at the base of the brittle crust [*Collettini and Barchi*, 2003].

[40] The observation of seismicity in the hanging wall of the principal normal faults and its clustering on secondary subparallel faults with dominantly normal faulting mechanisms underscores the complexity of this sequence which cannot be explained solely in terms of fault segmentation. Block rotation models [*Jackson and White*, 1989], for instance, have been proposed to explain the activation of subparallel structures as a consequence of the ongoing extension and possibly as an antithetic system of a master low angle normal fault [*Lister and Davis*, 1989]. It is interesting to note that the three main events (two on 26 September and 14 October) of the sequence nucleated very close to the intersection between the compressional and the extensional structures [see also *Chiarabba and Amato*, 2003; *Collettini and Chiaraluce*, 2000] suggesting that the presence of a shallow basement influenced both the former compression and the present-day extension. The Umbria-Marche 1997 seismicity occurs in the upper Mesozoic cover on a relatively low angle SW dipping normal fault system which could be antithetic to the ATF low angle normal fault. Therefore the base of this shallow seismogenic layer (7–8 km) should coincide with the top of the metamorphic basement and/or the ATF, which could act as a basal decollement of the extensional deformation.

[41] This discussion emphasizes the relevance of fault interaction in such a complex normal fault system. *Cocco et al.* [2000] investigated fault interaction through static stress transfer for the six largest earthquakes of the sequence and concluded that, while Coulomb stress can explain the occurrence of subsequent normal faulting events along the Apenninic direction, it cannot explain the occurrence of seismicity with normal faulting in the hanging wall of the main fault planes. In Figure 12b we have shown in a vertical cross section the fault plane solutions associated to the earthquakes located in the central portion of the aftershock area (see the map in Figure 12a). Figure 12b clearly shows the presence of a subparallel secondary plane activated during the aftershock sequence with numerous normal faulting events. The similarity of the focal mecha-

nisms of hanging wall seismicity with those of the largest magnitude earthquakes implies that these events are consistent with the remote tectonic stress field active in the focal volume, even if they are not explained by coseismic stress transfer. These results suggest that the whole seismogenic volume was in close-to-failure conditions at the beginning of the sequence and that the fractional stress drop was small. The slip heterogeneity on the main shock fault planes should also be taken into account to interpret the pattern of seismicity at very close distances. The slip gradient on the fault plane would create a stress gradient in the hanging wall where seismicity is observed. These considerations explain why we observe aftershocks in the hanging wall of the main faults but not in the footwall. However, other mechanisms such us fluid flow or structural complexities could play an important role in explaining the aftershock pattern and the response to the main shock induced stress perturbations.

[42] **Acknowledgments.** We thank Alessandro Amato, Giulio Selvaggi, Davide Piccinini, Maurizio Ripepe, Marco Cattaneo, Barbara Castello, Anne Deschamps, Massimo Di Bona, Paolo Mangano, and Alberto Michelini, for helpful discussion and collaborations in data processing and analyses. We are indebted to Felix Waldhauser, David P. Schaff, and Andy Michael for providing the codes used in the relocation analysis and stress field investigations. We also thank Stephanie Prejan, Alessandro Pino, and Luca Valensise for reviewing a preliminary version of the paper. We appreciated the review of J. Jackson and two anonymous reviewers, who allowed us to improve the manuscript. We benefited of the accurate work in processing the data of many researchers of INGV Rome, University of Camerino and University of Nice Sophia Antipolis, who participated in the field experiments and acquisition campaign. This research has been partially supported by the EC contract ENV-CT1-1999-00001 project Presap. Lauro Chiaraluce was supported by EC funds within the Presap project.

## References

Amato, A., et al., The 1997 Umbria-Marche, Italy, earthquake sequence: A first look at the main shocks and aftershocks, *Geophys. Res. Lett.*, *25*, 2861–2864, 1998.

Bally, A. W., L. Burbi, C. Cooper, and R. Ghelardoni, Balanced sections and seismic reflection profiles across the central Apennines, *Mem. Soc. Geol. It.*, *35*, 257–310, 1986.

Barchi, M. R., Lithological and structural controls on the seismogenesis of the Umbria region: Observations from seismic reflection profiles, *Bull. Soc. Geol. It., Spec.* Vol. 1, 855–864, 2002.

Barchi, M., A. De Feyter, B. Magnani, G. Minelli, G. Pialli, and B. M. Sotera, The structural style of the Umbria-Marche fold and thrust belt, *Mem. Soc. Geol. It.*, *52*, 557–578, 1998.

Barchi, M., F. Galadini, G. Lavecchia, P. Messina, M. Michetti, L. Peruzza, A. Pizzi, E. Tondi, and E. Vittori, Sintesi delle conoscenze sulle faglie attive in Italia centrale: Parametrizzazione ai fini della caratterizzazione della pericolosità sismica, report, Cons. Naz. delle Ric., Gruppo Naz. per la Difesa dai Terremoti, Rome, 2000.

Basili, R., and M. Meghraoui, Coseismic and postseismic displacements related with the 1997 earthquake sequence in Umbria-Marche (central Italy), *Geophys. Res. Lett.*, *28*, 2695–2698, 2001.

Boncio, P., and G. Lavecchia, A geological model for the Colfiorito earthquakes (September–October 1997, central Italy), *J. Seismol., Special Issue*, *4*, 345–356, 2000.

Boncio, P., F. Brozzetti, and G. Lavecchia, Architecture and seismotectonics of a regional low-angle normal fault zone in central Italy, *Tectonics*, *19*, 1038–1055, 2000.

Braunmiller, J., and J. Nàbelek, Geometry of continental normal faults: Seismological constraints, *J. Geophys. Res.*, *101*, 3045–3052, 1996.

Braunmiller, J., J. Nàbelek, and B. Leitner, The 1993 Klamath Falls, Oregon, earthquake sequence: Source mechanisms from regional data, *Geophys. Res. Lett.*, *22*, 105–108, 1995.

Calamita, F., and A. Pizzi, Recent and actives extensional tectonics in the southern Umbro-Marchean Apennines, *Mem. Soc. Geol. It.*, *48*, 541–548, 1994.

Calamita, F., M. Coltorti, D. Piccinini, P. P. Pierantoni, A. Pizzi, M. Ripepe, V. Scisciani, and E. Turci, Quaternary faults and seismicity in the Umbro-Marchean Apennines (central Italy): Evidence from the 1997 Colfiorito earthquake, *J. Geod.*, *29*, 245–264, 2000.

Capuano, P., A. Zollo, A. Emolo, S. Marcucci, and G. Milana, Rupture mechanism and source parameters of Umbria-Marche mainshocks from strong motion data, *J. Seismol., Special Issue*, *4*, 463–478, 2000.

Cattaneo, M., et al., The Umbria-Marche (Italy) earthquake sequence: Analysis of the data recorded by the local and temporary networks, *J. Seismol., Special Issue*, *4*, 401–414, 2000.

Cello, G., G. Deiana, L. Ferelli, L. Marchegiani, L. Maschio, S. Mazzoli, A. Michetti, L. Serva, E. Tondi, and T. Vittori, Geological constraints for earthquake faulting studies in the Colfiorito area (central Italy), *J. Seismol.*, Special Issue, *4*, 357–364, 2000.

Chiarabba, C., and A. Amato, $V_p$ and $V_p/V_s$ images in the $M_w$ 6.0 Colfiorito fault region (central Italy): A contribution to understand seismotectonic and seismogenic processes, *J. Geophys. Res.*, *108*(B5), 2248, doi:10.1029/2001JB001665, 2003.

Cinti, F. R., L. Cucci, F. Marra, and P. Montone, The 1997 Umbria-Marche (Italy) earthquake sequence: Relationship between ground deformation and seismogenic structure, *Geophys. Res. Lett.*, *26*, 895–898, 1999.

Cinti, F. R., L. Cucci, F. Marra, and P. Montone, The 1997 Umbria-Marche earthquakes (Italy): Relation between the surface tectonic breaks and the area of deformation, *J. Seismol.*, *4*(4), 333–343, 2000.

Cocco, M., C. Nostro, and G. Ekström, Static stress changes and fault interaction during the 1997 Umbria-Marche earthquake sequence, *J. Seismol., Special Issue*, *4*, 501–516, 2000.

Collettini, C., Architecture, geometry and mechanics of seismogenic normal faults in the northern Apennines, Ph.D. thesis, 199 pp., Univ. of Perugia, Perugia, Italy, 2001.

Collettini, C., and M. R. Barchi, A low angle normal fault in the Umbria region (central Italy): Mechanical model for the related microseismicity, *Tectonophysics*, in press, 2003.

Collettini, C., and L. Chiaraluce, A fluid-dependent seismogenic model as possible explanation of the evolution of the Umbria-Marche 1997 seismic sequence (central Italy), *Eos Trans. AGU*, *81*(48), Fall Meet. Suppl., Abstract H71C-13, 2000.

D'Agostino, N., J. A. Jackson, F. Dramis, and R. Funicello, Interactions between mantle upwelling, drainage evolution and active normal faulting: An example from the central Apennines (Italy), *Geophys. J. Int.*, *147*, 475–497, 2001.

Deschamps, A., D. Iannaccone, and R. Scarpa, The Umbrian earthquake (Italy) of 19 September 1979, *Ann. Geophys.*, *2*, 29–36, 1984.

Deschamps, A., et al., Spatio-temporal distribution of seismic activity during the Umbria-Marche crisis, 1997, *J. Seismol., Special Issue*, *4*, 377–386, 2000.

Ekström, G., A. Morelli, E. Boschi, and A. M. Dziewonski, Moment tensor analysis of the central Italy earthquake sequence of September–October 997, *Geophys. Res. Lett.*, *25*, 1971–1974, 1998.

Frechét, J., Sismogenése et doublets sismiques, thése d'Etat, 206 pp., Univ. é Sci. et Méd. de Grenoble, Grenoble, France, 1985.

Frepoli, A., and A. Amato, Contemporaneous extension and compression in the northern Apennines from earthquake fault-plane solutions, *Geophys. J. Int.*, *129*, 368–388, 1997.

Got, J. L., J. Frechét, and F. W. Klein, Deep fault plane geometry inferred from multiplet relative relocation beneath the south flank of Kilauea, *J. Geophys. Res.*, *99*, 15,375–15,386, 1994.

Haessler, H., R. Gaulon, L. Rivera, R. Console, M. Frogneux, G. Gaparini, L. Martel, G. Patau, M. Siciliano, and A. Cisternas, The Perugia (Italy) earthquake of 29, April 1984: A microearthquake survey, *Bull. Seismol. Soc. Am.*, *78*, 1948–1964, 1988.

Hernandez, B., F. Cotton, M. Campillo, M. Courboulex, M. Cocco, and S. Stramondo, Rupture history of the 1997 Umbria-Marche (central Italy) largest earthquakes from inversion of GPS, SAR and near field seismological data (abstract), *Eos Trans. AGU*, *80*(46), Fall Meet. Suppl., F739, 1999.

Hunstad, I., M. Anzidei, M. Cocco, P. Baldi, A. Galvani, and A. Pesci, Modeling coseismic displacements during the 1997 Umbria-Marche earthquake, *Geophys. J. Int.*, *139*, 283–295, 1999.

Hunstad, I., G. Selvaggi, N. D'Agostino, P. England, P. Clarke, and M. Pierozzi, Geodetic strain in peninsular Italy between 1875 and 2001, *Geophys. Res. Lett.*, *30*(4), 1181, doi:10.1029/2002GL016447, 2003.

Ichinose, G. A., J. Zeng, J. G. Anderson, and K. D. Smith, Modeling aftershocks of the 17 May 1993 $M_w$ 6 Eureka Valley earthquake (abstract), *Eos Trans. AGU*, *79*(46), Fall Meet. Suppl., F660, 1998.

Jackson, J. A., and N. J. White, Normal faulting in the upper continental crust: Observations from regions of active extension, *J. Struct. Geol.*, *11*, 15–36, 1989.

Jolivet, L., et al., Midcrustal shear zone in postorogenic extension: Example from the northern Tyrrhenian Sea, *J. Geophys. Res.*, *103*, 12,123–12,160, 1998.

Keller, J. V. A., and G. Pialli, Tectonics of the Island of Elba: A reappraisal, *Boll. Soc. Geol. It.*, *109*, 423–425, 1990.

Keller, J. V. A., G. Minelli, and G. Pialli, Anatomy of a late orogenic extension: The northern Apennines case, *Tectonophysics*, *238*, 275–294, 1994.

Lister, G. S., and G. A. Davis, The origin of metamorphic core complexes and detachment faults formed during Tertiary continental extension in the northern Colorado River region, U.S.A., *J. Struct. Geol.*, *11*, 65–94, 1989.

Mariucci, M. T., A. Amato, and P. Montone, Recent tectonic evolution and present stress in the northern Apennines (Italy), *Tectonics*, *18*, 108–118, 1999.

Massonet, D., and K. Feigl, Satellite radar interferometric map of the coseismic deformation field of the $M = 6.1$ Eureka Valley, California earthquake of May 17, 1993, *Geophys. Res. Lett.*, *22*, 1541–1544, 1995.

Meghraoui, M., V. Bosi, and T. Camelbeeck, Fault fragment control in the 1997 Umbria-Marche, central Italy, earthquake sequence, *Geophys. Res. Lett.*, *26*, 1069–1072, 1999.

Mendoza, C., and S. H. Hartzell, Aftershock pattern and mainshock faulting, *Bull. Seismol. Soc. Am.*, *78*, 1438–1449, 1988.

Michael, A., Determination of stress from slip data: Faults and folds, *J. Geophys. Res.*, *89*, 11,517–11,526, 1984.

Michael, A., W. L. Ellsworth, and D. H. Oppenheimer, Coseismic stress changes induced by the 1989 Loma Prieta, California, earthquake, *Geophys. Res. Lett.*, *17*, 1441–1444, 1990.

Michelini, A., D. Spallarossa, M. Cattaneo, A. Govoni, and A. Montanari, The 1997 Umbria-Marche (Italy) earthquake sequenze: Tomographic images obtained from data of the GNDT-SSN temporary network, *J. Seismol., Special Issue*, *4*, 415–433, 2000.

Mirabella, A., and S. Pucci, Integration of geological and geophysical data along a section crossing the region of the 1997–98 Umbria-Marche earthquakes (Italy), *Boll. Soc. Geol. It., Special*, *1*, 2001.

Paige, C. C., and M. A. Saunders, LSQR: An algorithm for sparse linear equations and sparse least squares, *ACM Trans Math. Software*, *8*, 43–71, 1982.

Piccinini, D., and CDC Working Group, A macroseismic study in a seismic gap: Città di Castello 2000 experiment, paper presented at European Geophysical Society Meeting, Nice, France, April 2002.

Pino, N. A., and S. Mazza, The Umbria-Marche (central Italy)earthquakes: Relation between rupture directivity and sequence evolution for the *Mw* > 5 shocks, *J. Seismol., Special Issue*, *4*, 451–461, 2000.

Pino, N. A., S. Mazza, and E. Boschi, Rupture directivity of the major shocks in the 1997 Umbria-Marche (central Italy) sequence from regional broadband waveforms, *Geophys. Res. Lett.*, *26*, 2101–2104, 1999.

Poupinet, G., W. L. Ellsworth, and J. Frechet, Monitoring velocity variations in the crust using earthquake doublets: An application to the Calaveras Fault, California, *J. Geophys. Res.*, *89*, 5719–5731, 1984.

Prejean, S., W. Ellsworth, M. Zoback, and F. Waldhauser, Fault structure and kinematics of the Long Valley Caldera Region, California, revealed by high-accuracy earthquake hypocenters and focal mechanism stress inversions, *J. Geophys. Res.*, *107*(B12), 2355, doi:10.1029/2001JB001168, 2002.

Ripepe, M., D. Piccinini, and L. Chiaraluce, Foreshock sequence of September 26th, 1997 Umbria-Marche earthquakes, *J. Seismol., Special Issue*, *4*, 387–399, 2000.

Rossetti, F., C. Faccenna, L. Jolivet, and R. Funicello, Structural evolution of the Giglio island, northern Thyrrenian Sea, *Mem. Soc. Geol. It.*, *52*, 493–512, 1998.

Rubin, A. M., D. Gillard, and J.-L. Got, Streaks of micro-earthquakes along creeping faults, *Nature*, *400*, 635–641, 1999.

Salvi, S., et al., Modeling coseismic displacements resulting from SAR interferometry and GPS measurements during the Umbria-Marche seismic sequence, *Journ. of Seismol.*, *4*, 479–499, 2000.

Schaff, D. P., 4D high resolution seismology: Repeating events and large scale relocation, Ph.D. thesis, 115 pp., Stanford Univ., Stanford, Calif., 2001.

Schaff, D. P., G. H. R. Bokelmann, G. C. Beroza, F. Waldhauser, and W. L. Ellsworth, High-resolution image of Calaveras Fault, California, seismicity, *J. Geophys. Res.*, *107*(B9), 2186, doi:10.1029/2001JB000633, 2002.

Shearer, P. M., Improving local earthquake locations using the L1 norm and waveform cross correlation: Application to the Whittier Narrows, California, aftershock sequence, *J. Geophys. Res.*, *102*, 8269–8283, 1997.

Waldhauser, F., hypoDD: A program to compute double-difference hypocenter locations, *U.S. Geol. Surv. Open File Rep., 01-113*, 2001.

Waldhauser, F., and W. L. Ellsworth, A double-difference earthquake location algorithm: Method and application to the northern Hayward Fault, California, *Bull. Seismol. Soc. Am.*, *90*, 1353–1368, 2000.

Waldhauser, F., and W. L. Ellsworth, Fault structure and mechanics of the Hayward fault, California, from double-difference earthquake locations, *J. Geophys. Res.*, *107*(B3), 2054, doi:10.1029/2001JB000084, 2002.

Zollo, A., S. Mariucci, G. Milana, and P. Capuano, The Umbria-Marche 1997 (central Italy) earthquake sequence: Insight on the mainshock rupture from near source strong motion records, *Geophys. Res. Lett.*, *26*, 3165–3169, 1999.

C. Chiarabba, L. Chiaraluce, and M. Cocco, Istituto Nazionale di Geofisica e Vulcanologia, Via di Vigna Murata 605, Rome, I-00143 Italy. (chiaraluce@ingv.it; cocco@ingv.it)

W. L. Ellsworth, U.S. Geological Survey, 345 Middlefield Road, MS 977, Menlo Park, CA 94025-3591, USA. (ellsworth@usgs.gov)